



**HAL**  
open science

## Adaptation to graviportality in Rhinoceroidea? An investigation through the long bone shape variation in their hindlimb

Christophe Mallet, Guillaume Billet, Raphael Cornette, Alexandra Houssaye

### ► To cite this version:

Christophe Mallet, Guillaume Billet, Raphael Cornette, Alexandra Houssaye. Adaptation to graviportality in Rhinoceroidea? An investigation through the long bone shape variation in their hindlimb. Zoological Journal of the Linnean Society, 2022, 10.1093/zoolinnean/zlac007. hal-03611156

**HAL Id: hal-03611156**

**<https://hal.science/hal-03611156>**

Submitted on 8 Jun 2022

**HAL** is a multi-disciplinary open access archive for the deposit and dissemination of scientific research documents, whether they are published or not. The documents may come from teaching and research institutions in France or abroad, or from public or private research centers.

L'archive ouverte pluridisciplinaire **HAL**, est destinée au dépôt et à la diffusion de documents scientifiques de niveau recherche, publiés ou non, émanant des établissements d'enseignement et de recherche français ou étrangers, des laboratoires publics ou privés.

1 **Adaptation to graviportality in Rhinocerotoida? An investigation through the**  
2 **long bone shape variation in their hind limb**

3

4 Christophe Mallet<sup>1</sup>, Guillaume Billet<sup>2</sup>, Raphaël Cornette<sup>3</sup>, Alexandra Houssaye<sup>1</sup>

5 1 Mécanismes adaptatifs et évolution (MECADEV), UMR 7179, MNHN, CNRS, 55 rue Buffon, CP 55,  
6 75005, Paris, France

7 2 Centre de Recherche en Paléontologie – Paris (CR2P), UMR CNRS 7207, MNHN, CNRS, SU, 8 rue  
8 Buffon, CP 38, 75005 Paris, France

9 3 Institut de Systématique, Evolution, Biodiversité (ISYEB), UMR 7205, MNHN, CNRS, SU, EPHE, UA,  
10 57 rue Cuvier, CP 50, 75005 Paris, France

11

12 Corresponding author:

13 Christophe Mallet

14 55 rue Buffon, CP 55, 75005, Paris, France

15 Email address: [christophe.mallet@edu.mnhn.fr](mailto:christophe.mallet@edu.mnhn.fr)

16

17 Running title: **Bone shape variation in the hindlimb of Rhinocerotoida**

18 **ABSTRACT**

19 Weight support is a strong functional constraint modelling limb bones in heavy quadrupeds.  
20 However, the complex relations existing between bone shape, mass, size and body proportions have  
21 poorly been explored. Rhinocerotidae is one of the groups showing the highest body mass reached  
22 by terrestrial mammals through time. Here, we explored the evolutionary variation of shape in hind  
23 limb stylopod and zeugopod bones and its relation with mass, size and gracility in this superfamily.  
24 Our results show that bones undergo a general increase of robustness towards high masses,  
25 associated with reinforcements of the main muscle insertions. The shape of the femur, carrying a  
26 marked phylogenetic signal, varies conjointly with mass, size and gracility, while that of the tibia  
27 appears related to gracility and mass only. The shape of the fibula does not vary according to those  
28 of the tibia. Moreover, congruent variation of shape between the distal part of the femur and the  
29 complete tibia underlines the potentially strong covariation of the elements constituting the knee  
30 joint. These results, coupled with those previously obtained on forelimb, allow a better  
31 comprehension of the relation between bone shape and mass among Rhinocerotidae, and a  
32 refining of the concept of “graviportality” in this superfamily.

33

34 **KEYWORDS**

35 Appendicular skeleton – Body mass – Brachypody – Functional morphology – Geometric  
36 morphometrics – Graviportality – Rhinoceros

## 37 INTRODUCTION

38 In quadrupeds, limb long bones, together with the muscles acting on them, fulfil essential functions  
39 like body support and locomotion (Hildebrand, 1974). Consequently, their shape is regarded as  
40 strongly related to variations of body size, body mass, as well as locomotor habits (Polly, 2007;  
41 Biewener & Patek, 2018). The convergent tendency of many quadruped lineages to reach high body  
42 mass across their evolution (Cope, 1887; Depéret, 1907; Raia *et al.*, 2012; Baker *et al.*, 2015; Bokma  
43 *et al.*, 2016) has led to repeated patterns of musculoskeletal constructions related to increase in size  
44 and mass. For more than a century, big animals have often been classified as “graviportal” and  
45 opposed to “cursorial” ones being characterized generally by smaller proportions (Hildebrand, 1974;  
46 Carrano, 1999). Skeletal features often associated with “graviportality” in tetrapods are columnar  
47 and thick limbs, vertically oriented girdle bones, changes in limb segment proportions (reduction of  
48 the autopodium and lengthening of the stylopodium) and an increase in bone compactness (Gregory,  
49 1912; Osborn, 1929; Hildebrand, 1974; Coombs, 1978; Eisenmann & Guérin, 1984; Biewener,  
50 1989a,b; Bertram & Biewener, 1990; Houssaye, Fernandez, & Billet, 2016). Limitations in locomotor  
51 habits have also been observed in “graviportal” animals, like the inability to gallop in elephants or  
52 hippos (Alexander & Pond, 1992). The different combinations of all these modifications lead to a high  
53 diversity of body plans associated with a single given body mass (Hildebrand, 1974; Polly, 2007).  
54 However, while higher body mass is expected to influence modifications of the bone shape itself in  
55 "graviportal" animals, the extent of those modifications is poorly studied among quadrupeds.

56 The Rhinoceroidea superfamily, only represented by five surviving species nowadays (Dinerstein,  
57 2011), was extremely diverse during the Cenozoic. More than 100 species have been described in  
58 Eurasia, North America and Africa, with a notable diversity of ecological niches and locomotor  
59 morphologies (Prothero & Schoch, 1989; Cerdeño, 1998; Prothero, 2005; Biasatti, Wang, & Deng,  
60 2018). Rhinoceroidea displayed an important variation in body mass, ranging from less than 100 kg  
61 in *Hyrachyus* Leidy, 1871, the most ancient representative of the superfamily (Antoine, 2002; Bai *et*  
62 *al.*, 2017), to more than 10 tons in giant Paraceratheriidae (Fortelius & Kappelman, 1993; Prothero,  
63 1998, 2013; Qiu & Wang, 2007) (Table 1). A convergent increase in body mass occurred in different  
64 lineages, in which many species frequently exceeded a body mass of one ton (Cerdeño, 1998).

65 Throughout their evolutionary history, rhinocerotoids also underwent drastic modifications of their  
66 general body plan (e.g., limb morphologies suggesting a transition from "cursorial" to "graviportal"),  
67 their degree of brachypody (or gracility, i.e., reduction of their relative limb length), their ecological  
68 affinities (from open environments to presumed semi-aquatic lifestyles), their number of forelimb  
69 digits (tetradactyl or tridactyl manus), the presence of horns and the relative size of their head  
70 (Guérin, 1989; Prothero & Schoch, 1989; Prothero, 1998, 2005, 2013; Cerdeño, 1998; Antoine, 2002;

71 Becker, 2003; Becker *et al.*, 2009; Bai *et al.*, 2017). All these parameters may therefore have covaried  
72 with the shape of their long bones.

73 As a consequence, given the diversity in body mass, size and proportions encountered in this group  
74 over more than 50 million years, this superfamily constitutes an excellent case study for the  
75 exploration of the evolution of long bone shape in relation with these morphological parameters.  
76 Only a few works previously explored the shape variation of the limb bones in modern or fossil  
77 rhinocerotoids, and in relation with mass, size or degree of brachypody / gracility (Guérin, 1980;  
78 Prothero & Sereno, 1982; Becker, 2003; Mallet *et al.*, 2019; Etienne *et al.*, 2020b; Mallet *et al.*, 2020).  
79 A recent integrative study explored this relationship between shape, size, mass and gracility on  
80 forelimb elements at the scale of the superfamily (Mallet *et al.*, in press). Beyond a common general  
81 increase of bone robustness towards high body mass in Rhinoceroidea, it also underlined that  
82 shape is not equally associated with size, mass and gracility among forelimb bones and that some  
83 groups (i.e., Paraceratheriidae, Teleoceratina) followed very different allometric trends compared to  
84 the rest of the superfamily. The shape variation patterns observed on the stylopodium followed  
85 more the evolutionary history than that observed on the zeugopodium. Moreover, the study of some  
86 partial anatomical areas highlighted that proximal and distal epiphyses varied in relation to size, mass  
87 and gracility in different ways to the variation observed across the entire bone (Mallet *et al.*, in  
88 press).

89 Building on these findings, our present study extends this approach to the hind limb elements.  
90 Previous results on modern rhinos (Mallet *et al.*, 2019, 2020) indicated congruent shape variation  
91 between fore- and hind limb stylopod elements (i.e., similar trends and high integration between the  
92 humerus and femur), with shape variation and covariation being likely more related to phylogeny  
93 than to body mass. Remarkable differences between fore- and hind limb zeugopod elements were  
94 also highlighted, with a stronger correlation of shape variation with body mass in the forelimb. These  
95 differences between fore- and hind limb elements may be related to divergent functional roles. Fore-  
96 and hind limbs do not act similarly during quadrupedal mammal locomotion, the former functioning  
97 as brakes and vital in directional change, the latter ensure body propulsion (Lessertisseur & Saban,  
98 1967; Heglund, Cavagna, & Taylor, 1982; Dutton *et al.*, 2006). Although all four limbs sustain the whole  
99 body mass, quadrupedal mammals bear a significantly higher part of their body mass on the  
100 forelimbs (Alexander, 1985; Henderson, 2006). This is particularly noticeable in rhinos, whose  
101 massive head, large muscle mass at the withers, and presence of horns in some species, are likely to  
102 increase the proportion of the total body mass carried by the forelimbs (Henderson, 1999; Regnault  
103 *et al.*, 2013; Stilson, Hopkins, & Davis, 2016; Panagiotopoulou, Pataky, & Hutchinson, 2019).  
104 However, even if the length of the fore- and hind limbs is relatively similar in most Rhinoceroidea

105 (Guérin, 1980), some taxa like Paraceratheriidae display a non-horizontal spine associated with  
106 having notably longer forelimbs than hindlimbs. This particular body plan likely changes which limbs  
107 support the largest part of the body mass and might also generate strong body mass-related shape  
108 variation on hind limbs elements, as it has previously been observed on ankle bones of Perissodactyla  
109 (Etienne *et al.*, 2020b).

110 The exploration of shape variation in the hind limb bones could help establish how body mass and its  
111 repartition across the animal is reflected in bone shape variation. Some similar trends as in the  
112 forelimb are likely to be observed, such as an increase of bone robustness towards high body mass  
113 (Mallet *et al.*, in press). However, relationships between shape variation and size, species mean body  
114 mass, and degree of gracility might not be equivalent between the different hind limb bones (femur,  
115 tibia and fibula). Moreover, the different roles of fore- and hind limbs in weight support (forelimb)  
116 and propulsion (hind limb) are predicted to be associated with notable differences in shape variation  
117 across Rhinoceroidea. Based on previous studies, we hypothesize: (a) strong congruences between  
118 the shape variation and mass, size and gracility in hind limb bones; (b) differences between  
119 stylopodial and zeugopodial elements in their patterns of shape variation with respect to size, mass  
120 and gracility, but also (c) between complete and partial bones; (d) a link between phylogeny and  
121 bone shape to be reflected in different ways for the three studied bones (after the results of Mallet  
122 *et al.*, 2019); (e) differences in trends of shape variation between the fore- and the hind limbs  
123 possibly related to their distinct functional roles.

## 124 MATERIAL AND METHODS

125 The studied sample was composed of 215 bones of modern and fossil species of Rhinoceroidea  
126 housed in fourteen institutions. The sample includes 79 femora, 83 tibiae and 53 fibulae (see  
127 Supplementary Table S1 for the complete list of studied specimens) representing 53 taxa (5 modern  
128 and 48 fossil species) belonging to almost all families of the superfamily Rhinoceroidea (no  
129 representative of the recently-defined family Eggyodontidae could be included) (Fig. 1). Taxa were  
130 selected to include as much body shape and mass diversity as possible and to cover the largest  
131 temporal range although this selection also depended greatly on the material availability. Taxonomic  
132 attributions were verified or updated using recent literature, directly with specimen numbers when  
133 available, or using taxonomic lists and institution databases for each locality. We retained the most  
134 recent binomial names considered as correct following the International Commission on Zoological  
135 Nomenclature rules (see Supplementary Table S1).

136 We selected adult individuals with fully fused epiphyses and retained only complete bones displaying  
137 no or negligible taphonomic effects (e.g., shallow surface cracks not altering the global shape). We  
138 rejected specimens massively crushed or restored with plaster. Following the results of Mallet *et al.*  
139 (in press) indicating potentially different results between complete and partial bones, we also  
140 considered incomplete bones in partial shape analyses (see below), as long as they were not crushed  
141 or distorted, in order to test if differences observed on forelimb bones may exist as well on hind limb  
142 bones. Very little information was available regarding sex for fossil specimens. Sexual dimorphism is  
143 known for some species and may slightly affect the shape of long bones (Guérin, 1980; Dinerstein,  
144 1991; Mead, 2000; Zschokke & Baur, 2002; Mihlbachler, 2007; Chen *et al.*, 2010). However, following  
145 Mallet *et al.* (2019), we assumed that this intraspecific variation should be largely exceeded by  
146 interspecific shape changes. We selected up to three specimens per bone for each species. All  
147 anatomical terms (illustrated in Supplementary Fig. S1) follow classic veterinary terminology and  
148 anatomical works on Perissodactyla or only on rhinoceroses (Guérin, 1980; Federative Committee on  
149 Anatomical Terminology, 1998; Antoine, 2002; Prothero, 2005; Barone, 2010a; Heissig, 2012; Bai *et al.*,  
150 2017). Locations of muscle insertions follows Etienne, Houssaye, & Hutchinson, 2021.

### 151 3D models

152 Most of the bones were digitized using a structured-light three-dimensional scanner (Artec Eva) with  
153 reconstructions with Artec Studio Professional (v12.1.1.12—Artec 3D, 2018). We also used this  
154 software to reconstruct bones broken in two or more pieces (without any missing part) in a single  
155 complete mesh. Nine specimens were digitized with a photogrammetric approach, following Mallison  
156 & Wings (2014) and Fau, Cornette, & Houssaye (2016). We used Agisoft Photoscan (v1.4.2—Agisoft,

157 2018) to reconstruct 3D models using sets of photos. Two specimens were digitized using medical  
158 computed tomography scanners at the Royal Veterinary College, London (Equine Hospital) and at the  
159 University of California, San Francisco (Department of Radiology & Biomedical Imaging). For these  
160 specimens, we extracted bone surfaces as meshes using Avizo (v9.5.0—Thermo Fisher Scientific,  
161 2018). As a few specimens displayed small lacking parts, mostly on the shaft, we used Geomagic  
162 Studio (v2014.3.0.1781—3D Systems Corporation, 2014) to fill holes. We used the “curvature filling”  
163 tool to ensure that the added polygons matched the curvature of the surrounding mesh. Finally, we  
164 decimated each mesh to reach 250,000 vertices and 500,000 faces using MeshLab (v2016.12—  
165 Cignoni *et al.*, 2008). We performed our analyses on left bones, mirroring right bones when left ones  
166 were unavailable.

### 167 **3D geometric morphometrics**

168 We analysed the shape variation of our sample through a 3D geometric morphometrics approach, a  
169 methodology widely used to quantify and visualize the morphological differences between objects by  
170 comparing the spatial coordinates of points called landmarks (Adams, Rohlf, & Slice, 2004; Zelditch *et*  
171 *al.*, 2012). We quantified the bone shape by placing a set of anatomical landmarks and curve and  
172 surface sliding semi-landmarks on the meshes, following Gunz & Mitteroecker (2013) and Botton-  
173 Divet *et al.* (2016). We placed anatomical landmarks and curves on meshes using IDAV Landmark  
174 (v3.0—Wiley *et al.*, 2005). The geometric location of landmarks and sliding semi-landmarks is derived  
175 from previous morphometric works on rhinoceros long bones (Mallet *et al.*, 2019, 2020) to cover the  
176 shape diversity of the sample (see Supplementary Data S1 for details on landmark numbers and  
177 locations). We created a template to automate the placement of surface sliding semi-landmarks for  
178 each bone. We chose a specimen [*Dicerorhinus sumatrensis* (Fischer, 1814) NHMUK ZE 1948.12.20.1]  
179 to be the initial specimen on which all anatomical landmarks, curve and surface sliding semi-  
180 landmarks were placed. We selected this individual for its average shape and size ensuring that all  
181 points would be correctly projected on other bones despite the great shape and size ranges of the  
182 sample. This specimen was then used as template for the projection of surface sliding semi-  
183 landmarks on the surface of all other specimens. Projection was followed by a relaxation step to  
184 ensure that projected points matched the actual surface of the meshes. We then slid curve and  
185 surface sliding semi-landmarks to minimize the bending energy of a thin plate spline (TPS) between  
186 each specimen and the template at first, and then four times between the result of the previous step  
187 and the Procrustes consensus of the complete dataset. Therefore, all landmarks could be treated at  
188 the end as geometrically homologous (Gunz, Mitteroecker, & Bookstein, 2005; Gunz & Mitteroecker,  
189 2013).



190 As we chose to work at the species level, we then computed and analysed species mean shapes  
191 (Botton-Divet *et al.*, 2017; Serio, Raia, & Meloro, 2020). After the sliding step, we computed a first  
192 Generalized Procrustes Analysis (GPA) with all specimens to remove the effect of size, location and  
193 orientation of the different landmark conformations (Gower, 1975; Rohlf & Slice, 1990). Then we  
194 computed the Procrustes consensus (or mean shape) of each species in the same geometric space.  
195 We superimposed these Procrustes consensus in a second GPA in order to pool all species means  
196 in a single morphospace. We repeated this process for each bone separately. As our dataset  
197 contained more variables than observations, we computed a Principal Component Analysis (PCA) to  
198 reduce dimensionality (Baylac & Frieß, 2005; Gunz & Mitteroecker, 2013) and visualize the  
199 distribution of the species in the morphospace. We also computed theoretical shapes associated  
200 with both minimum and maximum of the first two components of PCAs using a Thin-Plate Spline  
201 (TPS) deformation of the meanshape of our sample in each case. Theoretical shapes have also been  
202 used to produce colour maps of the location and intensity of the shape deformation between  
203 maximal and minimal values of regression: for each bone, the shape associated with the minimum  
204 values was coloured depending on its distance to the shape associated with the maximum values.  
205 We then plotted phylogenetic relationships between taxa (see below) in the morphospace. In order  
206 to visualize the whole shape variation, we computed Neighbour Joining (NJ) trees on all PC scores  
207 and compared it to the results of the PCAs on the two first PC scores. We performed projection,  
208 relaxation, sliding processes, GPAs, PCAs and theoretical shape computation using the “Morpho”  
209 package (v2.8—Schlager, 2017) in the R environment (v3.5.3—R Core Team, 2014). We plotted  
210 phylogeny on the morphospace using the “geomorph” package (v3.2.1—Adams & Otárola-Castillo,  
211 2013). We computed NJ trees using the “ape” package (v5.3—Paradis *et al.*, 2018a).

## 212 **Analyses on partial bones**

213 Our observations on fossil long bones of rhinoceros showed that redundant breakage patterns were  
214 observable due to various taphonomic agents throughout diagenesis (e.g., high sedimentary pressure  
215 on weak anatomical areas, scavenger action on marrow-rich parts – see Guérin, 1980; Hullot &  
216 Antoine, 2020). As on the forelimb (Mallet *et al.*, in press), some parts of the hind limb bones were  
217 often damaged or absent in fossil specimens. This was notably the case on the femur, where the  
218 femoral head, the third trochanter, the medial lip of the trochlea and the condyles were frequently  
219 too damaged to be included in shape analyses.

220 To overcome these taphonomic problems and include as many relevant specimens as possible (i.e.,  
221 cover the broadest range of body mass and size as possible), we performed analyses on isolated  
222 proximal and distal parts of the femur, using the same protocol as described in Mallet *et al.* (in

223 press). Following Bardua *et al.* (2019), we used curve sliding semi-landmarks to define artificial lines  
224 acting as a limit for the sliding of surface semi-landmarks and virtually remove damaged or missing  
225 parts from analyses. These limit lines involved at least one anatomical landmark to ensure that they  
226 were geometrically homologous on all specimens. We placed them as well on complete bones, which  
227 were all included in the analyses on partial bones. We finally removed limit lines after the sliding  
228 process and before the GPA to consider only true biological shape information in our analyses. We  
229 used two datasets on partial bones, for the proximal and distal halves of the femur, respectively (see  
230 Supplementary Information Data S1 for details on landmarks and sliding semi-landmarks in templates  
231 of partial bones).

### 232 **Phylogenetic framework**

233 Recent publications refined the phylogenetic relationships within Rhinoceroidea (Wang *et al.*,  
234 2016; Tissier *et al.*, 2018; Tissier, Antoine, & Becker, 2020; Bai *et al.*, 2020) and within Ceratomorpha  
235 (Bai *et al.*, 2020), although not including all genera of rhinocerotoids currently known worldwide.  
236 Therefore, no comprehensive and consensual phylogeny of the whole superfamily Rhinoceroidea  
237 exists to date. To take into account the effect of phylogeny on shape variation, we constructed a  
238 composite cladogram using trees previously computed on cranio-dental and postcranial characters or  
239 molecular data. We reconstructed interspecific relationships, branch lengths and occurrence dates  
240 after the works of Cerdeño (1995), Antoine (2002), Antoine, Duranthon, & Welcomme (2003),  
241 Antoine *et al.* (2010), Prothero (2005), Boada-Saña (2008), Piras *et al.* (2010), Becker, Antoine, &  
242 Maridet (2013), Lu (2013), Wang *et al.* (2016), Averianov *et al.* (2017), Tissier *et al.* (2018), Tissier,  
243 Antoine, & Becker (2020), Bai *et al.* (2020). We used the cladistic framework of Antoine *et al.* (2003)  
244 and Becker *et al.* (2013) to define families, subfamilies, tribes and subtribes (Fig. 1). To date, the  
245 relationships between the five modern taxa remain controversial, especially regarding the position of  
246 the Sumatran rhinoceros (*Dicerorhinus sumatrensis*) and its extinct relatives (e.g., Tougaard *et al.*,  
247 2001; Orlando *et al.*, 2003; Fernando *et al.*, 2006; Price & Bininda-Emonds, 2009; Steiner & Ryder,  
248 2011; Yuan *et al.*, 2014; Welker *et al.*, 2017; Cappellini *et al.*, 2019; Antoine *et al.*, 2021). These  
249 uncertainties are likely due to a hard polytomy at the base of the crown-group containing the five  
250 modern species (Willerslev *et al.*, 2009; Gaudry, 2017). Although recent genomic analyses tend to  
251 indicate that African and Asiatic rhinos constitute two sister-groups (Liu *et al.*, 2021), we considered a  
252 hard polytomy in our analyses and we addressed phylogenetic uncertainties using a NNI procedure  
253 (see below).

254 To address the effect of phylogenetic relationships on shape data for each bone, we evaluated their  
255 phylogenetic signal by computing a multivariate K statistic ( $K_{\text{mult}}$ ) on PC scores (Adams, 2014). This

256 index compares the rate of observed morphological change with that expected under a Brownian  
257 motion model on a given phylogeny (Blomberg *et al.*, 2003; Adams, 2014). As the  $K_{mult}$  computation  
258 requires fully bifurcating trees, we removed polytomies using the function *multi2di* in the “ape”  
259 package (Paradis *et al.*, 2018). This function resolves polytomies by randomly creating a new branch  
260 with a null length from one branch of the polytomous node (Swenson, 2014; Paradis *et al.*, 2018). We  
261 then computed  $K_{mult}$  values using the function *K.mult* in the “phylocurve” package (Goolsby, 2015).

## 262 **Body mass, centroid size and gracility index**

263 As in Mallet *et al.* (in press) for the forelimb, we addressed the relation of three variables related to  
264 body proportions and size – body mass, centroid size of the bone, and gracility index – with the  
265 shape of each long bone of the hind limb within Rhinoceroidea. We retrieved mean body mass  
266 (BM) of each species from the literature, compiling up to three estimations per species to compute  
267 mean BMs (see Table 1 and Supplementary Table S2). However, BM estimations can be highly  
268 heterogeneous for a single species depending on the considered method and morphological proxy  
269 (mostly on dental and cranial measurements, and less frequently on postcranial ones), the specimen  
270 developmental stage, or the geological formation. Moreover, equations for BM estimation were  
271 rarely developed taking into account Perissodactyla or rhinoceroses, resulting in potentially biased  
272 results for fossil Rhinoceroidea (Prothero & Sereno, 1982). We managed to collect BM estimation  
273 for only 34 of the 53 taxa constituting our sample. Consequently, we also consider the centroid size  
274 (CS) of each bone, which is classically used to address allometric variation, i.e. the shape variation  
275 linked to size (Zelditch *et al.*, 2012; Mitteroecker *et al.*, 2013; Klingenberg, 2016; Hallgrímsson *et al.*,  
276 2019). CS is defined as the square root of the sum of the square of the distance of each point to the  
277 centroid of the landmark set (Zelditch *et al.*, 2012). CS is known to be a good proxy of the mass of the  
278 animal (Ercoli & Prevosti, 2011; Cassini, Vizcaíno, & Bargo, 2012), notably for limb bones of  
279 rhinoceros (Mallet *et al.*, 2019; Etienne *et al.*, 2020b). In addition, given the large range of body  
280 shapes within Rhinoceroidea (Fig. 1) and the fact that the same mass can be associated with both a  
281 slender or a robust body condition, we used the mean gracility index computed on the third  
282 metatarsal (GI-MT3) as an estimator of the degree of brachypody of the hind limb (see Table 1 and  
283 Supplementary Table S2). This index is computed dividing the transverse width of the third  
284 metatarsal by its maximal length and has been used widely in rhinocerotoid studies, together with  
285 the same index computed on the third metacarpal for the forelimb (Colbert, 1938; Arambourg, 1959;  
286 Guérin, 1980; Cerdeño, 1998; Becker, 2003; Becker *et al.*, 2009; Scherler *et al.*, 2013). Among  
287 Rhinoceroidea, the higher the GI-MT3 value, the shorter the pes length: species with a high GI-MT3  
288 value are considered as more brachypodial (or less gracile) than species with low values. We  
289 computed this index by measuring third metatarsals when available in collections or compiling up to

290 three GI-MT3 values in the literature to compute mean GI-MT3. These metatarsals were mostly  
291 associated with long bones for modern species, and mostly associated with a similar locality for fossil  
292 species (Supplementary Table S2). We addressed the effect of phylogeny on log-transformed CS, log-  
293 transformed cubic root of the mean BM, and log-transformed mean GI-MT3 using the univariate K  
294 statistic (Blomberg *et al.*, 2003). We tested for correlation between these three variables respectively  
295 using a linear regression on Phylogenetic Independent Contrasts (Felsenstein, 1985). We used the  
296 function *contMap* of the “phytools” package (Revell, 2012) to plot these three variables along the  
297 phylogeny.

298 Variation patterns, notably covariation, can be analysed at different levels: across species  
299 (evolutionary variation), within a species at a single developmental stage (static variation), within a  
300 species across developmental stages (ontogenetic variation) (Klingenberg, 2014). Here, we  
301 investigated the evolutionary covariation of bone shape with each of the three variables (BM, CS, GI-  
302 MT3) considering a multivariate approach using Phylogenetic Generalized Least Squares (PGLS), a  
303 regression model taking into account the phylogenetic framework and computed here on Procrustes  
304 coordinates to quantify the shape variation related to CS, BM and GI-MT3 (Martins & Hansen, 1997;  
305 Rohlf, 2001; Klingenberg & Marugán-Lobón, 2013; Adams & Collyer, 2018). We used the function  
306 *procD.pgls* (with 1,000 iterations) of the “geomorph” package (v3.2.1—Adams & Otárola-Castillo,  
307 2013), suited for 3D geometric morphometric data. As the function *procD.pgls* uses a Brownian  
308 Motion model of evolution to compute PGLS, which assumes non-directional trait changes, other  
309 models might assume a different computational hypothesis. To account for these changes depending  
310 on the considered model, we also computed PGLS under a Phylogenetic Ridge Regression model of  
311 evolution (Castiglione *et al.*, 2018). The Phylogenetic Ridge Regression allows to take into account  
312 variations of evolutionary rates along the different branches of a phylogenetic tree, accounting for  
313 potential accelerations and decelerations of the phenotypic changes among groups in a more  
314 accurate way than does a Brownian Motion model. We therefore used the function *PGLS\_fossil* of  
315 the ‘RRphylo’ package (v.2.5.0 – Castiglione *et al.*, 2018) to compute PGLS with a Ridge Regression  
316 model and compare it to the results obtained under a Brownian Motion model in order to see  
317 whether our results were robust to model variations.

318 As previously mentioned, the phylogeny of Rhinoceroidea remains debated for both extant and  
319 extinct taxa and is frequently renewed by the determination of new representatives (Tissier *et al.*,  
320 2020; Bai *et al.*, 2020). Consequently, we assessed the effect of potential uncertainty in taxa position  
321 in the phylogeny on PGLS by using a Nearest Neighbour Interchange (NNI) procedure. NNI algorithm  
322 generates new trees by swapping two adjacent branches of a specified tree (Felsenstein, 2004). We  
323 generated new trees using the *nni* function of the package “phangorn” (Schliep, 2011) and computed

324 PGLS with these rearranged trees to estimate the ranges of  $R^2$  and p-values. It should be noted that  
325 the  $R^2$  value of a PGLS can hardly be compared with that of an ordinary least squares regression (Ives,  
326 2019; Billet & Bardin, 2021). Consequently, our interpretations of data will rely as little as possible on  
327 these  $R^2$  values alone.

328 We considered all statistical tests as significant for p-values  $\leq 0.01$ . However, given that recent works  
329 call for a continuous approach of the p-value (Wasserstein, Schirm, & Lazar, 2019; Ho *et al.*, 2019),  
330 we chose to mention results having a p-value up to 0.05 as well.

## 331 RESULTS

### 332 Correlation between BM and GI-MT3

333 Both mean BM and mean GI-MT3 carry a significant phylogenetic signal ( $K_{BM} = 1.75$ ,  $p < 0.01$ ;  $K_{GI-MT3} =$   
334  $1.08$ ,  $p < 0.01$ ) but are only marginally correlated to each other when taking into account  
335 phylogenetic relationships ( $p = 0.06$ ). The evolution of both parameters along the phylogeny (Fig. 2)  
336 highlights that the evolution of these parameters within the superfamily is decoupled in some taxa  
337 like Paraceratheriidae, Teleoceratina and, at a lesser extent, large Elasmotheriinae.

### 338 Differences in PGLS between Brownian Motion and Phylogenetic Ridge Regression

339 Very similar results were obtained between PGLS computed under a Brownian Motion model (using  
340 the geomorph functions) and under a Phylogenetic Ridge Regression (RR) model (using the RRphylo  
341 functions) (see Supplementary Table S3 for detailed comparison between models). Significant  
342 regressions under a BM model remain significant under a RR model, as well as non-significant results  
343 under a Brownian Motion model remain non-significant under a RR model. We note very low  
344 variations of  $R^2$ ,  $p$ -values and shape deformations between the two models. Only regression plots  
345 show marked differences, with a much higher spread of specimens in those obtained under a RR  
346 model, making their interpretation more difficult. For these reasons, we will present only results  
347 obtained under a Brownian Motion model in the following sections.

### 348 Femur – complete bone

349 Shape data for the complete femur carry a strong phylogenetic signal ( $K_{mult} = 0.93$ ,  $p < 0.01$ ). The  
350 distribution of the species both in the NJ tree (Fig. 3A) and in the phylomorphospace (Fig. 4) is  
351 strongly reminiscent of the phylogenetic relationships between taxa. Along the NJ tree, Hyrachyidae  
352 group with Hyracodontidae, Elasmotheriinae (all of small size in the absence of *Elasmotherium*  
353 Fischer, 1808) and some Rhinocerotinae [*Protaceratherium* Forster-Cooper, 1911 and *Peraceras* [Pe.]  
354 *profectum* (Matthew, 1899)]. *Paraceratherium* Forster-Cooper, 1911 groups with two species of  
355 *Aphelops* Cope, 1874 while *Metamynodon* Scott & Osborn, 1887 is close to some Aceratheriini  
356 (*Hoploaceratherium* Ginsburg & Heissig, 1989) as well as some Rhinocerotina (*Lartetotherium*  
357 Ginsburg, 1974). While Aceratheriini are dispersed along the tree, most of the Rhinocerotina are  
358 grouped together. Similarly, Teleoceratina form a homogeneous cluster despite the presence of  
359 *Peraceras* [Pe.] *hessei* Prothero & Manning, 1987. Conversely, *Chilotherium* Ringström, 1924 and  
360 *Pleuroceros* Roger, 1898, two highly brachypodial taxa, plot within Rhinocerotina, far from other  
361 brachypodial species like *Teleoceras* Hatcher, 1894. On the phylomorphospace, the first two axes  
362 gather 58.4% of the global variance. PC1, which carries 42.9% of the variance, displays a structure

363 similar to the general organisation of the NJ tree. Small taxa such as *Hyrachyus* and *Hyracodon* Leidy,  
364 1856 plot toward positive values. Towards moderately negative values, small Elasmotheriinae plot  
365 near *Metamynodon*, *Trigonias* Lucas, 1900 and small Aceratheriini. The giant paraceratheriid  
366 *Urtinotherium* Chow & Chiu, 1963 plots near small taxa like *Trigonias* or *Protaceratherium*, but also  
367 near *Metamynodon*. Towards the most negative values, large Aceratheriini are mixed with  
368 Teleoceratina and Rhinocerotina. Along PC2, which carries 15.5% of the variance, Rhinocerotina form  
369 a homogeneous cluster plotting towards negative values, together with *Metamynodon*, *Hyrachyus*  
370 and *Subhyracodon* Brandt, 1878. Teleoceratina and Aceratheriini (except *Aphelops* [Ap.]  
371 *malacorhinus* Cope, 1878) group together with *Urtinotherium*, *Subhyracodon mitis* (Cope, 1875) and  
372 *Hyracodon* towards positive values.

373 The shape variation along PC1 is mainly related to the bone robustness (Fig. 4 and Supplementary  
374 Fig. S2A). Less negative values are associated with a slender bone showing a rounded hemispherical  
375 head with a narrow neck; a proximally developed greater trochanter tuberosity protruding over the  
376 head; an oval *fovea capitis*; a third trochanter situated at the first proximal third of the shaft, more  
377 developed caudally than laterally; a cranio-caudally straight shaft; a relatively symmetrical distal  
378 trochlea with a poorly developed medial lip; a long and narrow trochlear groove running caudally to  
379 the shaft; a distal epiphysis showing a medial torsion relatively to the shaft; relatively symmetrical  
380 medial and lateral condyles. Conversely, negative values are associated with a thick and massive  
381 bone, with a general hourglass shape in cranial view; a more flattened and wide head with a large  
382 neck; a greater trochanter tuberosity poorly developed proximally and not protruding over the head;  
383 a small rounded *fovea capitis*; a strong third trochanter clearly protruding laterally and cranially from  
384 the shaft; a shaft slightly curved in the caudal direction; a strongly asymmetrical trochlea with a  
385 broad medial lip; a short and wide trochlear groove; a distal epiphysis oriented cranially relatively to  
386 the shaft; a medial condyle more developed than the lateral one. Along PC2, the shape variation  
387 mostly concerns the development of the trochanters and the relative proportions of the epiphyses.  
388 The theoretical shape associated with negative values shows proximal and distal epiphyses of similar  
389 medio-lateral width; a lesser trochanter situated just below the head and above the third trochanter  
390 on the opposite side; a third trochanter developed in both cranial and lateral directions. Conversely,  
391 the shape associated with positive values displays a head and greater trochanter relatively larger; a  
392 head oriented more proximally; lesser and third trochanters facing each other on the medial and  
393 lateral side of the shaft, respectively; a third trochanter reduced to a bony ridge; a medial lip of the  
394 trochlea more developed cranially.

395 The centroid size of the complete femur bears a significant phylogenetic signal ( $K_{CS} = 1.05$ ,  $p < 0.01$ )  
396 and is significantly correlated with BM ( $r = 0.70$ ,  $p < 0.01$ ) but not with GI-MT3 ( $p = 0.37$ ) (Table 2).

397 PGLS results indicate that shape is significantly correlated with CS, BM and GI-MT3. PGLS computed  
398 on NNI trees highlight that variations in phylogenetic relationships may result in marginally non-  
399 significant correlations for CS and GI-MT3 but mean p-values are strongly significant (Table 3). In the  
400 regression plot of shape against CS, the distribution of taxa shows a relatively poor fit to the  
401 regression line. Small taxa like *Hyrachyus*, *Hyracodon* and small Elasmotheriinae plot above the  
402 regression line together with *Metamynodon*, some Aceratheriini and Rhinocerotina. *Paraceratherium*  
403 plots far above the regression line. Teleoceratina are all grouped below the line together with most  
404 of Rhinocerotina (Fig. 5A). Hyrachyidae, Hyracodontidae, Arynodontidae and Paraceratheriidae  
405 seem to follow an independent path parallel to the Rhinocerotidae one, but as these groups have  
406 few representatives here, this observation must be taken with caution. Changes in CS values mainly  
407 affect the general robustness of the bone, which is slightly increased in larger femora. It also affects  
408 the greater trochanter tuberosity and convexity, the femoral head and particularly the *fovea capitis*.  
409 Along the shaft, the main changes are located on the lateral part between the greater trochanter  
410 convexity and the third trochanter (where inserts the *m. vastus lateralis*), as well as along the distal  
411 half of the diaphysis, on cranial and caudal sides. Lateral and medial parts of both condyles are also  
412 strongly modified by CS variations (Fig. 5A and Supplementary Fig. S3A). The structure of the  
413 regression plot of shape against BM is partly similar to that obtained with CS, with a relatively poor fit  
414 to the regression line, mainly driven by *Hyrachyus* at the minimal BM values. *Hyrachyus* is clearly  
415 isolated from all other species that form a large cluster at high BM values (Fig. 5B). *Metamynodon*  
416 (Arynodontidae) plots outside this cluster and far above from the regression line. A variation of BM  
417 results in the modifications of the same anatomical areas as for CS, although to a stronger extent,  
418 particularly for the femoral head and the greater trochanter convexity. An increase of robustness is  
419 observed towards high BM values. Shape changes are also located along the lesser trochanter, the  
420 medial lip of the trochlea and the medial epicondyle (Fig. 5B and Supplementary Fig. S3B). The  
421 regression plot of shape against GI-MT3 indicates a good fit to the regression line, better than the  
422 two ones with CS and BM. We can observe a clear separation between Rhinocerotina, being almost  
423 all above the regression line at mid-GI-MT3 values, and most other species below the line at various  
424 GI-MT3 values. Hyrachyidae and Hyracodontidae isolated towards minimal values, together with  
425 *Menoceras* Troxell, 1921, while other small Elasmotheriinae group with *Paraceratherium*, *Trionias*  
426 and some gracile Aceratheriini and Rhinocerotina. Teleoceratina form a homogeneous cluster slightly  
427 isolated from other species (Fig. 5C). Like for BM and CS, variations of GI-MT3 are associated with  
428 changes in the bone robustness, but are also related to modifications located on both medial and  
429 lateral supracondylar areas where inserts the *m. gastrocnemius*. However, contrary to what it is  
430 observed with BM, the medial lip of the trochlea and the medial epicondyle are poorly modified with  
431 variations of GI-MT3 values (Fig. 5C and Supplementary Fig. S3C).



432 **Femur – proximal part**

433 Shape data for the proximal part of the femur carry a significant phylogenetic signal ( $K_{\text{mult}} = 0.62$ ,  $p <$   
434  $0.01$ ). The distribution of the species in the NJ tree (Fig. 3B) and in the phylomorphospace (Fig. 6A)  
435 shows marked differences with the results obtained on complete bones. The NJ tree is structured by  
436 the separation in three main clusters: 1) Hyrachyidae, Hyracodontidae, small Elasmotheriinae  
437 together with one rhinocerotine *incertae sedis (i. s.) (Protaceratherium)* and one aceratheriine (*Pe.*  
438 *profectum*), 2) almost all Rhinocerotina together with *Pleuroceros*, and 3) Aceratheriini, Teleoceratina  
439 and Paraceratheriidae, together with *Metamynodon* and *Trigonias*. A similar structure is observed in  
440 the phylomorphospace, where the two first axes carry 62.1% of the total variance. PC1, which  
441 gathers 42.2% of the variance, mainly highlights the opposition between giant Paraceratheriidae on  
442 positive values and Rhinocerotina on negative values. PC2 gathers 19.9% of the variance and mainly  
443 separates small taxa (*Hyrachyus*, *Hyracodon*, small Elasmotheriinae, *Protaceratherium*, *Pe.*  
444 *profectum*) towards negative values from all other species towards positive values. *Metamynodon*  
445 and *Aphelops megalodus* occupy the highest positive values along this axis.

446 Along PC1, shape variation is mostly related to the general orientation of the proximal part relative  
447 to the rest of the bone and the development and position of the trochanters (Fig. 6A and  
448 Supplementary Fig. S2B). Towards negative values, the proximal part of the femur is tilted medially,  
449 with a relatively flattened head; a poorly developed greater trochanter tuberosity; a lesser  
450 trochanter placed directly below the femoral neck and above the third trochanter along the shaft; a  
451 third trochanter strongly extended cranially and laterally. Towards positive values, the proximal part  
452 of the femur is more vertical, with a rounded head supported by a thick neck; a greater trochanter  
453 tuberosity developed proximally and caudally; a long lesser trochanter situated in front of the third  
454 trochanter along the shaft; a third trochanter almost absent and reduced to a bony rugosity. Along  
455 PC2, the shape associated with negative values is long and slender, with a rounded head oriented  
456 proximo-medially; a high greater trochanter tuberosity; a short lesser trochanter; a long and poorly  
457 laterally developed third trochanter. The shape associated with positive values shows a flattened  
458 head oriented proximally; a low greater trochanter tuberosity; a long lesser trochanter; a third  
459 trochanter developed laterally and cranially.

460 As for the complete bones, CS of the proximal femur carries a strong phylogenetic signal ( $K_{\text{CS}} = 1.86$ ,  $p$   
461  $< 0.01$ ) and is strongly correlated with BM ( $r = 0.91$ ,  $p < 0.01$ ) but not with GI-MT3 ( $p = 0.18$ ) (Table  
462 2). Similarly, PGLS regressions indicate a significant correlation between shape and the three  
463 variables. NNI procedure highlights that some phylogenetic uncertainties can lead to marginally non-  
464 significant results (Table 3). The regression plot of shape against CS displays a poor fit to the

465 regression line, with a high dispersion of specimens. Almost all Rhinocerotina are below the  
466 regression line, only associated with Rhinocerotinae *i. s.*, *Trigonias*, *Subhyracodon* (Elasmotheriinae)  
467 and *Aphelops* (Aceratheriini). Above the regression line, Aceratheriini and Teleoceratina group  
468 together with *Metamynodon* (Aminodontidae), while Hyrachyidae and Hyracodontidae also plot well  
469 above the line at low CS values. Giant Paraceratheriidae plot far above the regression line at high CS  
470 values. They do not seem to follow the same allometric trend as other rhinocerotoids in the present  
471 case, and their presence probably pulled the regression line upwards at high CS values (Fig. 7A). The  
472 regression plot of shape against BM also displays a relatively poor fit to the regression line.  
473 *Hyrachyus* and *Paraceratherium* are isolated from most other taxa at extreme CS values and plot far  
474 above the regression line. Again, almost all Rhinocerotina, situated below the line, are separated  
475 from other species situated above the line (Fig. 7B). Contrary to the results obtained on complete  
476 bones, the regression plot of shape against GI-MT3 shows a more scattered dispersion of the species.  
477 There is also no clear preferential direction shown by the overall distribution of all specimens, which  
478 highlights a relatively poor fit to the regression line. Like for CS and BM, Rhinocerotina clearly isolate  
479 on one side of the regression line (above in this case) while almost all other species plot on the other  
480 side (far below for Paraceratheriidae, Hyrachyidae and *Teleoceras proterum* [Leidy, 1885]) (Fig. 7C).  
481 As for complete bones, shape variation associated with changes in CS and BM values impacts similar  
482 anatomical areas: mainly the greater trochanter tuberosity, the lesser trochanter and the cranial side  
483 of the shaft. However, the increase of robustness towards high values is not clear. The intensity of  
484 shape variation is slightly higher for BM than CS (Fig. 7A, B and Supplementary Fig. S3D, E). The shape  
485 changes associated with variations of GI-MT3 values mainly concern the femoral head, the lesser and  
486 third trochanters and the insertion area of the *m. vastus lateralis* (Fig. 7C and Supplementary Fig.  
487 S3F).

#### 488 **Femur – distal part**

489 The phylogenetic signal carried by shape data for the distal part of the femur is strong and significant  
490 ( $K_{\text{mult}} = 1.06$ ,  $p < 0.01$ ). The distribution of the species in the NJ tree (Fig. 3C) and in the  
491 phylomorphospace (Fig. 6B) differs noticeably from those obtained on the complete bone and  
492 proximal part. The NJ tree depicts an opposition between gracile and brachypodial taxa, with a poor  
493 influence of phylogenetic relationships: only Rhinocerotina group almost all together, despite the  
494 presence of Aceratheriini and Teleoceratina close to them. This sorting along the degree of  
495 brachypody is also observed on the phylomorphospace (especially PC1), where the first two axes  
496 gather 64.6% of the global variance (Fig. 6B). Along PC1, which carries 56.2% of the variance,  
497 *Hyrachyus* and *Hyracodon* plot together around null values, close to giant Paraceratheriidae and  
498 *Metamynodon*. Small Elasmotheriinae, *Trigonias* and *Protaceratherium* are mixed with relatively

499 gracile Aceratheriini, Rhinocerotina and Teleoceratina while the most brachypodial taxa (*Teleoceras*,  
500 *Chilotherium*, *Pleuroceros*) plot towards the maximal positive values, together with some *Dihoplus*  
501 Brandt, 1878, *Ceratotherium* Gray, 1868 and *Diceros* Gray, 1821. PC2, which gathers 8.2% of the  
502 variance, mainly opposes small Elasmotheriinae and *Protaceratherium* towards negative values to  
503 giant Paraceratheriidae and *Metamynodon* towards positive values. However, no clear pattern is  
504 visible regarding other taxa between these two extremes.

505 As for complete bones, the shape variation along PC1 is mainly related to the general robustness of  
506 the bone (Fig. 6B and Supplementary Fig. S2C). Theoretical shape associated with negative values  
507 displays a long and slender shaft; a narrow symmetrical trochlea developing caudally towards the  
508 condyles; symmetrical medial and lateral condyles. Conversely, the shape associated with positive  
509 values shows a robust and thick shaft, compressed proximo-distally; an asymmetrical trochlea with a  
510 massive medial lip; a medial condyle more developed than the lateral one; a protruding medial  
511 epicondyle. Along PC2, the shape associated with negative values has a narrower shaft; a medial lip  
512 of the trochlea poorly developed in the cranial direction; a narrow and deep V-profiled trochlear  
513 groove; medial and lateral condyles developed in the caudal direction. Conversely, the shape  
514 associated with positive values shows a more robust shaft; a medial lip of the trochlea which is more  
515 developed in the cranial direction; a wide and shallow trochlear groove; medial and lateral condyles  
516 which are poorly developed in the caudal direction.

517 The centroid size of the distal femur carries a significant phylogenetic signal ( $K_{CS} = 0.91$ ,  $p < 0.01$ ) and  
518 is highly correlated with BM ( $r = 0.86$ ,  $p < 0.01$ ) but not with GI-MT3 ( $p = 0.32$ ) (Table 2). However,  
519 contrary to what is observed on the complete bone and proximal part, PGLS regressions are only  
520 significant between shape and GI-MT3 (and marginally between shape and CS depending on the tree  
521 configuration) (Table 3). The regression plot of shape against GI-MT3 is very similar to that observed  
522 on the complete femur and shows a relatively good fit to the regression line (Fig. 8). Almost all  
523 Rhinocerotina are above the regression line, together with *Trigonias*, *Protaceratherium* and  
524 *Menoceras*. Aceratheriini are dispersed on each side of the line, some being mixed with  
525 Rhinocerotina. Below the regression line, Teleoceratina are grouped together with Paraceratheriidae  
526 and *Metamynodon*, while Hyrachyidae and Hyracodontidae isolate below the line towards minimal  
527 GI-MT3 values (Fig. 8). As for complete bones, beyond a slight increase of robustness, the shape  
528 variation associated with variations of GI-MT3 values is mainly located on both medial and lateral  
529 supracondylar areas where inserts the *m. gastrocnemius* (Fig. 8 and Supplementary Fig. S3G).  
530 Although marginally non-significant, the regression plot of shape against CS displays a strong  
531 similarity with those obtained on the complete bone and proximal part, with a relatively weak fit to  
532 the regression line. We observe an opposition between almost all Rhinocerotina and Teleoceratina

533 below the regression line (together with Rhinocerotinae *i. s.*), and all other species above the line.  
534 Like in previous results, Aceratheriini are dispersed among this central cluster, while *Hyrachyus-*  
535 *Hyracodon* and giant Paraceratheriidae plot far away from the line at minimal and maximal CS values  
536 respectively. Similarly, the shape variation associated with changes of CS values mainly affects the  
537 third trochanter, the cranial side of the shaft and both medial and lateral condyles (see  
538 Supplementary Fig. S4A for regression plot and shape deformation).

### 539 **Tibia**

540 As was observed for the femur, shape data obtained on the tibia carry a significant phylogenetic  
541 signal ( $K_{\text{mult}} = 1.27$ ,  $p < 0.01$ ). The NJ tree is strongly structured by the degree of brachypody,  
542 opposing mainly Hyrachyidae to the most brachypodial species of Teleoceratina (Fig. 3D).  
543 Rhinocerotina plot almost all together. *Elasmotherium* and *Diaceratherium* Dietrich, 1931 plot within  
544 the Aceratheriini group, whereas all other Teleoceratina are isolated at an extremity of the tree.  
545 *Paraceratherium* is close to *Peraceras* Cope, 1880 and Rhinocerotina, but also of all other  
546 Aceratheriini. The first two axes of the phylomorphospace gather 78.0% of the total variance and  
547 display a structure similar to that of the NJ tree (Fig. 9A). PC1 carries 65.4% of the variance and is  
548 associated with bone robustness, with gracile tibiae occupying positive values and robust tibiae  
549 negative values. PC1 opposes Hyrachyidae and Hyracodontidae towards positive values to  
550 Teleoceratina towards negative values. Along this axis, small Elasmotheriinae plot next to  
551 Hyrachyidae and Hyracodontidae, together with *Protaceratherium*. Species with a larger tibia like  
552 *Elasmotherium* and *Paraceratherium* plot together with most of the Aceratheriini, the genus  
553 *Diaceratherium* and some Rhinocerotina. Taxa with a short and very robust tibia like *Teleoceras*,  
554 *Brachypotherium* Roger, 1904, *Prosantorhinus* Heissig, 1973 and *Pleuroceros* occupy the most  
555 negative values. PC2 carries 12.6% of the variance and mainly opposes Teleoceratina with a short and  
556 robust tibia towards negative values to some Rhinocerotina (with gracile tibia like *Stephanorhinus*  
557 Kretzoi, 1942, *Dicerorhinus* Gloger, 1841 and more robust ones like *Ceratotherium* and *Dihoplus*), as  
558 well as *Pe. profectum* and *Paraceratherium* towards positive values.

559 Shape variation along PC1 is mostly related to the general robustness of the bone (Fig. 9A and  
560 Supplementary Fig. S2D). Towards positive values, the tibia is thin and slender, with: a triangular  
561 tibial plateau tilted in the caudal direction and showing similar surface areas for the medial and  
562 lateral articular surfaces; a lateral surface area highly developed in the caudal direction towards the  
563 popliteal notch; medial and lateral intercondylar tubercles separated by a large gap; a small and flat  
564 tibial tuberosity associated with a narrow and deep tibial groove; a long and narrow shaft with  
565 relatively parallel medial and lateral edges; a distal articular surface for the fibula forming an

566 isosceles triangle; a narrow and asymmetrical articular surface for the astragalus, with a lateral  
567 groove deeper than the medial one; a caudal apophysis stretched caudally. Conversely, the  
568 theoretical shape associated with negative values is highly robust and thick, with: an irregular tibial  
569 plateau tilted medially and cranially; a medial articular surface wider than the lateral one; a lateral  
570 surface area poorly developed in the caudal direction towards the popliteal notch; medial and lateral  
571 intercondylar tubercles separated by a narrow gap; a strong and massive tibial tuberosity oriented  
572 laterally and associated with a wide and shallow tibial groove; a massive diaphysis displaying a  
573 narrowing at midshaft, conferring to the bone a hourglass aspect in cranial view; a distal articular  
574 surface for the fibula forming an equilateral triangle; a wide, shallow and relatively symmetrical  
575 articular surface for the astragalus. Along PC2, the shape variation mainly affects both epiphyses.  
576 Towards positive values, the tibia has high intercondylar tubercles, with the medial one being placed  
577 more cranially than the lateral one; both medial and lateral condyles being developed caudally  
578 defining a deep popliteal notch; a high tibial tuberosity; a straight interosseous crest; a long distal  
579 articular surface for the fibula forming an isosceles triangle; a symmetrical articular surface for the  
580 astragalus; a medial malleolus developed distally. Conversely, towards negative values, the tibia has  
581 low intercondylar tubercles, both facing each other; medial and lateral condyles poorly developed  
582 caudally resulting in a narrow popliteal notch; a low tibial tuberosity; a rounded and concave  
583 interosseous crest; a short kidney-shaped distal articular surface for the fibula; an articular surface  
584 for the astragalus with a cranio-caudally tilted general axis; a medial malleolus poorly developed  
585 distally.

586 The centroid size of the tibia carries a significant although weak phylogenetic signal relative to the  
587 results obtained on the femur ( $K_{CS} = 0.56$ ,  $p = 0.01$ ). Similarly, CS is strongly correlated with BM ( $r =$   
588  $0.72$ ,  $p < 0.01$ ) but not with GI-MT3 ( $p = 0.14$ ) (Table 2). PGLS regressions are significant for BM and  
589 GI-MT3 only, although NNI procedure indicate that some tree configurations may led to significant  
590 results for CS as well (Table 3). The regression plot of shape against BM shares strong similarities with  
591 that obtained on the femur. Specimens show a rather good fit to the regression line with few  
592 outliers. Towards high BM values, there is a high dispersion of the species and a strong opposition  
593 between large Paraceratheriidae and some Teleoceratina on each side of the line. Conversely,  
594 Elasmotheriinae follow a trend parallel to the common regression line (Fig. 10A). The shape variation  
595 associated with changes of BM values is mostly located directly under the tibial plateau on the  
596 medial and lateral sides of the shaft, with a stronger intensity of shape variation in the former  
597 location. The tibial crest is also affected by shape changes of lesser intensity. The medial side of the  
598 tibial shaft is particularly affected by shape changes, especially proximally (Fig. 10A and  
599 Supplementary Fig. S3H). The regression plot of shape against GI-MT3 shows a good fit to the

600 regression line. This plot is very similar to that obtained on the femur, with the isolation of almost all  
601 Rhinocerotina above the regression line, only associated with *Elasmotherium*, *Paraceratherium* and  
602 *Aphelops*. Below the regression line, Hyrachyidae-Hyracodontidae, small Elasmotheriinae,  
603 Aceratheriini and Teleoceratina all form homogeneous groups separated from each other along GI-  
604 MT3 values (Fig. 10B). Towards high values of GI-MT3, shape variation involves an increase of  
605 robustness and a medio-lateral broadening of both epiphyses (Fig. 10B and Supplementary Fig. S3I).  
606 Shape variation is similar to that observed for changes in BM values, with a stronger general  
607 robustness and marked anatomical modifications located under the tibial plateau. These changes are  
608 mainly located on the proximal part of the medial side of the tibia, and distally to the tibial  
609 tuberosity. The distal part of the shaft is also affected, notably the distal articular surface for the  
610 fibula (see Supplementary Fig. S3 for shape deformation).

### 611 **Fibula**

612 The results obtained on the fibula differ strongly from those obtained on previous bones. Although  
613 significant, the phylogenetic signal carried by shape data is almost equal to 1 ( $K_{\text{mult}} = 0.99$ ,  $p < 0.01$ ),  
614 indicating a negligible influence of phylogenetic relations on the shape of the fibula. The distribution  
615 of the species on the NJ tree (Fig. 3D) and on the phylomorphospace (Fig. 9B) strongly differs from  
616 those obtained for the femur and the tibia. The NJ tree is mainly structured by an opposition  
617 between Teleoceratina, *Hyrachyus* and *Menoceras* on the one hand and Rhinocerotinae *i. s.*,  
618 Aceratheriini, Paraceratheriidae and Rhinocerotina strongly mixed together on the other hand. The  
619 first two axes of the phylomorphospace, gathering 76.0% of the global variance, reflect a similar  
620 structure to the NJ tree (Fig. 9B). PC1, accounting for 47.2% of the variance, opposes *Hyrachyus*,  
621 *Menoceras* and almost all Teleoceratina in the negative part to all other species on the positive part.  
622 Rhinocerotina, Aceratheriini and Rhinocerotinae *i. s.* form a cluster with no obvious structure.  
623 *Paraceratherium* plots near small taxa like *Protaceratherium* and *Peraceras*, but also near *Pleuroceros*  
624 and *Aphelops*. PC2, which gathers 28.8% of the variance, is mainly driven by an opposition between  
625 *Hyrachyus* and *Menoceras* towards positive values and *Teleoceras* towards negative values. Along  
626 this axis, while Rhinocerotina plot mainly with Teleoceratina, *Paraceratherium* is close to small taxa  
627 like *Menoceras*, *Plesiaceratherium* Young, 1937 and *Protaceratherium*. Aceratheriini are mixed  
628 together with Rhinocerotinae *i. s.*, Rhinocerotina and poorly brachypodial Teleoceratina.

629 Contrary to what was observed for the femur and the tibia, the shape variation along PC1 is less  
630 related to a change in the general robustness of the bone than along PC2 (Fig. 9B and Supplementary  
631 Fig. S2E). The shape associated with positive values is thin with a small rounded proximal articular  
632 surface for the tibia oriented cranially; a very thin central shaft with a sharp interosseous crest; a

633 long distal articular surface for the tibia forming an isosceles triangle; a medio-laterally flattened  
634 distal epiphysis; both cranial and caudal tubercles of the lateral malleolus being oriented caudally; a  
635 symmetrical kidney-shaped articular surface for the astragalus. Conversely, the shape associated  
636 with negative values is massive and thick with a large proximal articular surface for the tibia oriented  
637 more medially; a strong central shaft with a smooth interosseous crest; a very short distal articular  
638 surface for the tibia forming an equilateral triangle; a medio-laterally broadened distal epiphysis;  
639 both cranial and caudal tubercles of the lateral malleolus oriented laterally; an asymmetrical kidney-  
640 shaped articular surface for the astragalus. Surprisingly, the shape variation along PC2 also involves a  
641 huge change in robustness more marked than along PC1 and associated with morphological changes  
642 of both epiphyses. The shape associated with positive values is extremely thin and flat, with a spoon-  
643 like proximal articular surface for the tibia; a straight and flat shaft; a distal epiphysis with a caudal  
644 development conferring it a squared shape; a small rectangular articular surface for the astragalus.  
645 The shape associated with negative values is extremely thick and massive with a large proximal  
646 articular surface for the tibia; a strong shaft with a cranio-caudal curvature; a triangular and thick  
647 distal epiphysis; a kidney-shaped articular surface for the astragalus.

648 Contrary to what is observed in other bones, the centroid size of the fibula does not carry a  
649 significant phylogenetic signal ( $p = 0.22$ ). CS is highly correlated with BM ( $r = 0.71$ ,  $p < 0.01$ ) but not  
650 with GI-MT3 ( $p = 0.17$ ) (Table 2). As for the distal femur, PGLS regressions are only significant  
651 between shape and GI-MT3 (and marginally between shape and CS depending on the tree  
652 configuration) (Table 3). However, the regression plot of shape against GI-MT3 indicates a poor fit to  
653 the regression line, with many species plotting far away from the line (Fig. 10C). Rhinocerotina are  
654 almost all grouped above the regression line at mid-GI-MT3 values, while Teleoceratina are grouped  
655 below the line at high GI-MT3 values. *Aceratheriini* plot near Rhinocerotinae *i. s.* and  
656 *Paraceratherium* in the central cluster while *Hyrachyus* (Hyrachyidae) and *Menoceras*  
657 (Elasmotheriinae) isolate towards minimal GI-MT3 values, well below the line. The shape variation  
658 associated with changes of GI-MT3 values mainly involves morphological modifications of the caudal  
659 side of the fibula head, of the lateral part of the shaft and of the distal epiphysis, particularly the  
660 cranial and caudal tubercles of the malleolus and the distal articular surface for the tibia (Fig. 10C and  
661 Supplementary Fig. S3J). PGLS regression between shape and CS is non-significant at the considered  
662 threshold of  $p < 0.01$  (Table 3). The regression plot indicates a very weak fit to the regression line.  
663 *Paraceratherium* appears to strongly drive the regression trend being the only taxon with high CS  
664 values (see Supplementary Fig. S4B for regression plot). The shape variation associated with a higher  
665 CS involves mainly the same anatomical areas than those described for the shape variation related to  
666 GI-MT3 (see Supplementary Fig. S4B for shape deformation).

667 **Evolution of CS values along the phylogeny**

668 The evolution of CS values along the phylogeny for the distal femur (being that with the least amount  
669 of missing data), complete tibia and complete fibula (Fig. 11) highlights important disparities  
670 between the three bones. The distribution of CS values for the tibia is particularly distinct from those  
671 observed on the femur and the fibula. This distinction is notably due to *Teleoceratina*, showing very  
672 low values of CS for the tibia. On the fibula, the lowest values are not represented by *Hyrachyus* but  
673 by *Teleoceras*. Despite missing taxa for the fibula, most CS values for other taxa seem congruent with  
674 the distribution observed for the distal femur.

675



676 **DISCUSSION**

677 **Association of mass, size and gracility with bone shape**

678 *Congruent shape variation associated with all variables*

679 While it is never significantly correlated either with CS or BM, the gracility index GI-MT3 is always  
680 significantly correlated with shape variation for the femur, tibia and fibula. CS is always significantly  
681 and strongly correlated with body mass. However, this significant relationship between CS and BM  
682 should be considered carefully prior to interpretation, since CS values can be very different (or even  
683 very similar) between taxa depending on the considered bone. This is particularly obvious when  
684 comparing *Hyrachyus* and *Teleoceras*, which display similar values of CS for the tibia and the fibula  
685 (Fig. 11), whereas the mass of the former taxon was around ten times lower than that of the latter.  
686 The relationship between CS and BM is supported by stronger statistical results for the femur, for  
687 which size, mass and shape vary in a more congruent way. These results can also be partially related  
688 to the fact that CS is computed using the distance of each landmark to the centroid of the object:  
689 consequently, a long and thin object can have a similar CS value than a short and robust one, as it  
690 seems to be the case between *Hyrachyus* and *Teleoceras*. The poor correlation between CS and BM  
691 for the zeugopodial elements of the hind limb highlight the limitations of considering CS as a proxy  
692 for BM; the stronger relationship between CS and BM for the stylopod is also seen for the forelimb  
693 more so than for the hind limb. (see below and Mallet *et al.*, in press).

694 *Femur*

695 For the femur, a higher size, mass, or degree of brachypody is always associated with an increase of  
696 the general bone robustness, which is coherent with previous observations on rhinos (Prothero &  
697 Sereno, 1982; Mallet *et al.*, 2019; Etienne *et al.*, 2020b). Moreover, the variation of these variables is  
698 associated with that of many similar anatomical areas on the femur, though not always with the  
699 same intensity.

700 The femoral head is particularly affected by an increase of size, mass, or brachypody, especially for  
701 the two latter variables (Figs. 4 and 5). The shape and orientation of the femoral head change when  
702 these parameters increase, becoming more flattened and proximally oriented. This is likely to  
703 indicate a reorientation of the limb (and of its rotation axis), being more vertical and placed closer to  
704 the parasagittal axis of the animal when size, weight or brachypody increase. This conformation is  
705 classically associated with a “graviportal” body plan (Gregory, 1912; Osborn, 1929) and its presence  
706 in giant Paraceratheriidae confirm that their hip joint is oriented more distally with a femur placed  
707 close to the parasagittal plane (Prothero, 2013). However, such reorientation is also present in lighter

708 and more brachypodial species like Teleoceratina. This highlights the fact that characters classically  
709 associated with graviportality, like the reorientation of the femoral head, can be present in taxa  
710 displaying very different Bauplan layouts (see below).

711 Along the femoral shaft, high-intensity shape changes are observed at muscle origination points,  
712 which is highlighted more clearly in comparisons of shape with body mass and with brachypody (Figs.  
713 5B and C). Such changes are notably observed in Rhinocerotina for the insertion of the *m. vastus*  
714 *lateralis* (between the greater trochanter convexity and the third trochanter) and on both medial and  
715 lateral supracondylar tuberosities, where insert the *m. gastrocnemius* and digit flexors. These  
716 powerful muscles are respectively the main extensors of the zeugopodium and autopodium (Etienne  
717 *et al.*, 2021). Differences in bone shape associated with muscle attachments as organisms increase in  
718 mass or brachypody are coherent with more powerful muscles ensuring the propulsion and support  
719 of a higher absolute weight or of a body with a lower centre of gravity. Moreover, we observed that  
720 the bones of a brachypod species often form shorter lever arms than in dolichopod species (i.e., an  
721 animal having long limbs). Consequently, at equal mass, muscles will need to produce more power to  
722 apply higher forces on these shorter lever arms and ensure efficient movements and body support  
723 (McGhee & Frank, 1968; Hildebrand, 1974; Fischer & Blickhan, 2006).

724 On the distal epiphysis, an increase of CS, BM and GI-MT3 is also always associated with more  
725 asymmetrical trochlea and condyles. The asymmetry of the distal epiphysis, previously observed on  
726 modern rhinos (Mallet *et al.*, 2019), but also in equids (Hermanson & MacFadden, 1996) and bovids  
727 (Kappelman, 1988), is likely associated with the need to resist higher constraints exerted near the  
728 sagittal plane in taller and heavier quadrupeds. Surprisingly, this asymmetry seems poorly correlated  
729 with the thickening of the medial lip of the trochlea, related to body mass increase only (see below).

### 730 Tibia

731 Contrary to what is observed in the femur, shape variation in the tibia is only significantly correlated  
732 with the degree of brachypody and the body mass. On this bone, an increase of both body mass and  
733 brachypody is associated with an increase of the general robustness, as well as broader epiphyses.  
734 The tibial plateau is clearly wider for high values of BM and GI-MT3 (Figs. 9A and 10). The same  
735 observation can be made for the distal epiphysis, since the contact surface with the astragalus is  
736 wider, which is coherent with a medio-lateral enlargement of this bone previously observed among  
737 heavy Rhinocerotidea (Etienne *et al.*, 2020b). Similar epiphyseal broadenings have also been  
738 observed in heavy bovids (Etienne *et al.*, 2020a). Such proximal and distal broadenings likely confer a  
739 better resistance to the knee and ankle joints by ensuring the dissipation of loading forces due to a  
740 higher mass on a larger surface area. Moreover, most of the shape changes common to high mass

741 and brachypody are situated distally to the proximal epiphysis and involves the tibial fossa, the tibia  
742 crest and the lateral side of the shaft. These changes seem to be more strongly linked to brachypody  
743 than to body mass (Fig. 10). These areas constitute the insertion sites of powerful flexor muscles,  
744 respectively the *m. tibialis cranialis*, a foot flexor, and the *mm. biceps femoris, popliteus*,  
745 *semitendinosus* and *sartorius*, all being flexors of the leg (Etienne *et al.*, 2021). Reinforcement of  
746 insertions for flexors and extensors are congruent with the higher forces needed to move a heavier  
747 body.

#### 748 Fibula

749 The shape variation of the fibula is only significantly correlated with the degree of brachypody (and  
750 marginally with the centroid size), making it similar to what has been observed for the distal part of  
751 the femur (see below). However, no clear increase of robustness is related to an increase of  
752 brachypody. Morphological changes mainly involve the head and the proximal part of the shaft,  
753 where insert flexor and extensor muscles for digits. The distal part, on which the tendons of these  
754 muscles run and which is linked to ankle bones by the collateral ligament, is also affected by shape  
755 changes (Antoine, 2002; Fisher, Scott, & Adrian, 2010; Etienne *et al.*, 2021). Variations of the centroid  
756 size and degree of brachypody are accompanied by similar shape changes (i.e., larger bones have  
757 larger muscle insertion sites), although these two parameters are not significantly correlated. This  
758 indicates that similar shape changes may occur in the fibula of taxa showing different body shapes.

#### 759 *Non-congruent shape variation*

760 Although many shape changes of a given bone appear similarly related to variation of size, mass and  
761 brachypody, other morphological modifications can be more directly related to one specific  
762 parameter. This is notably the case of the *fovea capitis* on the femoral head, which is only associated  
763 with changes in centroid size. This fovea, where inserts the foveal ligament, may be almost absent in  
764 some rhino species like the modern black rhinoceros or the giant *Paraceratherium*. The disappearing  
765 of the fovea might be interpreted as the absence of this ligament (Crelin, 1988). However, a previous  
766 analysis on the elephant hip indicated that this ligament can be present despite the absence of fovea  
767 and attached on the distal ridge of the femoral head (Crelin, 1988). This fossa is present in various  
768 taxa, independently of their body mass, their locomotor ecology or their habitat: for example, in  
769 bovids (Etienne *et al.*, 2020a), in many carnivorans (Jenkins & Camazine, 1977), in porcupines (Yilmaz,  
770 1998) and even in most archosaurs (Tsai & Holliday, 2015). The functional role of the foveal ligament  
771 is poorly known, but is hypothesised to limit the abduction of the femur and prevent the dislocation  
772 of the hip joint (Crelin, 1988; Barone, 2010b). Consequently, the shape change associated with an  
773 increase of centroid size may not be due to the disappearing of this ligament but to the displacement

774 of its insertion on the femoral head, which could be related to higher constraints due to size or  
775 locomotor behaviour to prevent the hip dislocation if the leg deviates too much from the parasagittal  
776 plane during locomotion. However, this *fovea* is also absent or poorly marked in non-related and  
777 lighter taxa like *Diceros bicornis* (Linnaeus, 1758) (Guérin, 1980; Antoine, 2002), making it hard to  
778 relate its shape and presence or absence to a high body mass only. At the intraspecific level, this  
779 *fovea* can be more or less developed depending on the age of the specimen (Guérin, 1980; Mallet *et*  
780 *al.*, 2019). Consequently, our results do not allow a precise morphofunctional interpretation of the  
781 shape changes of this *fovea*, which remains to be explored more deeply among quadrupeds in  
782 relation with body proportions.

783 On the femur, all three trochanters modify strongly in association with an increase of CS, BM or GI-  
784 MT3, but not always in the same way. An increase of mass and brachypody is associated with a  
785 lateral development of the greater trochanter convexity, where inserts the *m. gluteus minimus*, an  
786 extensor of the limb (Etienne *et al.*, 2021). Similarly, an increase of the centroid size is mostly  
787 associated with changes in the top of the greater trochanter tuberosity, where inserts the *m. gluteus*  
788 *medius*, considered as the main limb extensor (Etienne *et al.*, 2021). A higher centroid size is  
789 associated with a lower tuberosity developed more caudally. The lateral development of the greater  
790 trochanter convexity in heavy and brachypodial taxa and the caudal development of the greater  
791 trochanter tuberosity lengthen the lever arms laterally and caudally, allowing slower but more  
792 powerful extensions and increasing the mechanical advantage of muscles extending the limb  
793 (Hildebrand, 1974). The variation of body mass and brachypody is particularly related to the variation  
794 of the lesser trochanter, where inserts the *m. iliopsoas*, showing a distal displacement for heavier  
795 and more brachypodial species. To a lesser extent, the third trochanter, where inserts the *m. gluteus*  
796 *maximus*, displays the same distal displacement (with shape changes only associated with variation  
797 of gracility index). Both trochanters are then facing each other at midshaft in heavy and brachypodial  
798 taxa, constituting longer lever arms for muscles which provides gravitational support, a conformation  
799 often observed in heavy taxa (Hildebrand, 1974).

800 On the distal epiphysis of the femur, the asymmetry of the trochlea is associated with a broadening  
801 of the medial lip for high body mass only. This medial lip, also called medial trochlear ridge, is  
802 considered as indicating the presence of a “passive stay-apparatus” in various quadrupeds like  
803 equids, rhinos or bovids, allowing the animal to endure long periods of standing during feeding or  
804 resting times (Hermanson & MacFadden, 1996). The appearance of this feature, which emerged  
805 independently in different lineages (Janis *et al.*, 2012), is hypothesized to be related to habitat  
806 complexity (Kappelman, 1988) or to body mass (Hermanson & MacFadden, 1996). Although we did  
807 not test the hypothesis of a relation with habitat, results on fossil rhinocerotoids tend to support a

808 link between the development of the medial trochlear ridge and a high body mass, as this feature is  
809 present in all heavy taxa (in *Metamynodon*, large Paraceratheriidae and all heavy Rhinocerotidae  
810 exceeding a ton). This passive “lock” of the knee joint likely allows heavy rhinos to stand during  
811 feeding or resting times without spending too much energy to counteract gravity. Furthermore, a  
812 similar pattern has been observed on the forelimb, with the bicipital groove of the humerus being  
813 only associated with changes in body mass (Mallet *et al.*, in press). As the bicipital groove is also likely  
814 involved in a passive-stay apparatus for the forelimb (Hermanson & MacFadden, 1992), these  
815 particularly congruent results underline that the development of joint lock systems is directly related  
816 to an increase of body mass among Rhinoceroidea.

### 817 **Differences in stylopodium and zeugopodium shape changes with body proportions**

818 In accordance with the second hypothesis, the comparison of patterns of shape change clearly  
819 highlights that the stylopodium and the zeugopodium do not follow the same trends of  
820 morphological variations. Whereas the shape variation of the femur is conjointly related to size, mass  
821 and gracility index, that of the tibia appears more highly correlated to the degree of brachypody than  
822 to the body mass. The shape of the fibula appears related to the degree of brachypody only (and only  
823 marginally to size). Beyond the general increase of robustness undergone by the bones in heavy  
824 species, these strong differences tend to indicate a functional breakdown between the evolution of  
825 the stylopodium and zeugopodium among Rhinoceroidea, both in fore- and hind limbs (see below).  
826 Hallgrímsson, Willmore, and Hall (2002) and Young and Hallgrímsson (2005) hypothesized an increase  
827 in variation of limb elements along the proximo-distal axis, especially in quadrupeds, relating this  
828 phenomenon to postnatal processes like functional specialization under specific environmental  
829 constraints. Our results tend to confirm these observations among Rhinoceroidea at the  
830 evolutionary level, distal elements of the limb (tibia and fibula) varying more than proximal ones  
831 (femur). This decoupling might be related to a divergence in the role of these bones, the femur being  
832 more involved in flexion and extension movements of both hip and leg to ensure propulsion, while  
833 the tibia mainly ensures weight support and gives attachment for flexor and extensors muscles of the  
834 foot (together with the fibula). The weaker correlation of tibial shape with body mass than with the  
835 degree of brachypody tends to indicate that the shape of this bone is more related to the distribution  
836 of the weight in the body (i.e., position of the centre of gravity, muscles and other organs) than to  
837 the absolute body weight of the species. These results appear as partly contradictory to what has  
838 been observed in modern rhinos, where zeugopodial shape was more directly linked to body mass  
839 than stylopodium’s one (Mallet *et al.*, 2019, 2020). However, the five modern species only represent  
840 a small sample of the past diversity of Rhinoceroidea and belong to a subtribe showing an  
841 evolutionary trend different from that of the superfamily (see below). This emphasizes that, at the

842 scale of the whole superfamily, the degree of brachypody (and, consequently, the body mass  
843 repartition and the position of the centre of gravity) may be a major driver of the morphological  
844 changes of the hind limb zeugopodium. Conversely, body mass itself may have a more visible impact  
845 at a lower taxonomic level (Mallet *et al.*, 2019, 2020). A similar trend differentiating stylopodium and  
846 zeugopodium bones has been observed on forelimb elements of the superfamily (see Mallet *et al.*, in  
847 press, and below).

#### 848 **Modularity of the femur**

849 Beyond the strict distinction between the stylopodium and zeugopodium, the multiple investigations  
850 of the femur based on complete or partial bone analyses reveal that the shape variations of the  
851 whole bone, of the proximal and of the distal parts, respectively, do not exhibit the same relationship  
852 with size, mass and gracility index. The shape of the proximal part appears significantly correlated  
853 with size, mass and gracility index, similarly to that of the complete bone, but the species dispersions  
854 in the NJ trees, phylomorphospaces and regression plots for these two datasets highlight noteworthy  
855 differences. Small taxa like Hyrachyidae, Hyracodontidae, small Elasmotheriinae and Rhinocerotinae  
856 *i. s.* share marked morphological affinities with heavy Paraceratheriidae concerning the whole bone,  
857 but this is barely the case when looking at its proximal part only. This tends to indicate that the  
858 proximal part of the femur undergoes shape modification decoupled from the ones observed on the  
859 rest of the bone between these taxa. This pattern of shape variation appears as different from that  
860 observed on the humerus of Rhinocerotidae, where the functional signal was similar between the  
861 complete bone and its distal epiphysis (see below and Mallet *et al.* in press). The modifications of the  
862 femur notably concern the size and the shape of the trochanters, as well as the head orientation.  
863 Conversely, the shape variation of the distal part of the femur is more congruent with the ones of the  
864 tibia and fibula than with the whole femur (high correlation with the degree of brachypody, poor  
865 correlation with body mass and no correlation with centroid size). All these observations led us to  
866 consider that proximal and distal parts of the femur may represent different morphological modules,  
867 *i.e.*, anatomical units “*that [are] tightly integrated internally but relatively independent from other*  
868 *such modules*” (Klingenberg, 2008). The congruence between the shape variation of the distal femur  
869 and the tibia could indicate that the knee joint, with the inclusion of the patella, displays a modular  
870 organisation. Similarly, the shape of the proximal femur could covary with the pelvic bone, although  
871 this covariation has been proven weak or non-existent in other mammal groups like equids or  
872 marsupials (Hanot *et al.*, 2017; Martín-Serra & Benson, 2019). All these questions remain to be  
873 addressed among modern and fossil rhinos through relevant modularity test (Goswami & Polly, 2010;  
874 Klingenberg, 2014).

875 **Bone shape and phylogenetic legacy**

876 The differences in shape variation patterns between the stylopodium and the zeugopodium may be  
877 related to functional breakdowns between limb segments. In addition, and except for the fibula (see  
878 below), shape as well as size, mass, and gracility index carry a strong phylogenetic signal (see Results  
879 section). The shape variation of the complete femur remains very similar among each clade and does  
880 not converge with that of other clades. This likely underlines the importance of the evolutionary  
881 legacy on the morphological disparity of this bone. Such differences between clades are less clear for  
882 its distal part only, as well as for the tibia, for which some taxa show convergences in shape (e.g.,  
883 *Elasmotherium*, *Aphelops* and *Diaceratherium*). This tends to confirm previous observations among  
884 modern rhinos, indicating a stronger phylogenetic signal in the variation of the stylopodium than in  
885 that of the zeugopodium (Mallet *et al.*, 2019; 2020). A similar trend has also been observed in the  
886 forelimb (see below) (Mallet *et al.*, in press).

887 The fibula appears as an exception among these bones, as its shape and centroid size carry almost no  
888 phylogenetic signal. Among the superfamily, only the subtribe Teleoceratina display a relative shape  
889 homogeneity for the fibula. No clear link between the shape of the fibula and body mass can be seen  
890 within the superfamily either. These observations somewhat echo previous results on modern  
891 rhinos, which showed a puzzling intraspecific shape variation exceeding the interspecific variation for  
892 this bone (Mallet *et al.*, 2019). In addition, the proximal and distal contact surfaces of the fibula are  
893 variably fused with those of the tibia among specimens and species; this fusion may potentially be  
894 related to evolutionary legacy, to the high body mass of the concerned species, or to the ontogenetic  
895 stage of the individual (Antoine, 2002; Polly, 2007). However, the fusion between these two bones  
896 can be observed in very different taxa, such as *Ceratotherium*, *Teleoceras* or *Menoceras*, without any  
897 obvious trend linked to phylogeny or body mass. This fusion can slightly modify the shape of the  
898 fibula, notably the interosseous crest and the size and shape of the distal synostosis surface.  
899 Moreover, shape data show important differences between the patterns of variation of the tibia and  
900 fibula, suggesting some level of independence between these two bones, as previously observed in  
901 modern rhinos (Mallet *et al.*, 2020). The fibula therefore stands out from the other bones by the fact  
902 that its variation in shape shows no clear structure, and this at all the considered scales within the  
903 superfamily.

904 Beyond these general trends, some groups among the superfamily follow remarkably different  
905 tendencies in their shape variation. Giant Paraceratheriidae, despite their extreme size and mass,  
906 rarely possess a shape plotting far away from other Rhinoceroidea in the different morphospaces.  
907 In fact, their hind limb bones show surprising proximities with some Aceratheriini or Rhinocerotini.

908 This underlines that their extreme size and mass are not reflected in extreme shape conformations  
909 and, conversely, that taxa with very different body mass can share shape similarities. This proximity  
910 could be related to the general body plan of these species: Paraceratheriidae are known to retain a  
911 “cursorial” body plan with a relatively high degree of slenderness (Granger & Gregory, 1936;  
912 Prothero, 2013) and their limb bones seem more constrained by this general body organisation than  
913 by constraints due to high body weight support and propulsion.

914 Conversely, Teleoceratina is another group deviating from the general trend of shape variation  
915 common to the whole superfamily. Teleoceratina often constitute extremes of shape variation,  
916 particularly the zeugopodial bones of highly brachypodial taxa like *Teleoceras*. This high degree of  
917 brachypody is also encountered in phylogenetically distant genera like *Pleuroceros* and *Chilotherium*,  
918 leading to marked shape similarities, especially on the zeugopodium. This convergent condition  
919 might be related to particular developmental trends among these groups, leading to a shortening of  
920 the distal limb. Such a particular condition may be involved in functional roles specific to these  
921 groups, such as walking on soft and unstable grounds (Boada-Saña, Hervet, & Antoine, 2007) or even  
922 a semi-aquatic ecology, although this hypothesis seems unlikely given various works (MacFadden,  
923 1998; Mead, 2000; Muhlbachler, 2003; Prothero, 2005; Clementz, Holroyd, & Koch, 2008; Wang &  
924 Secord, 2020). Following these authors, larger foot could help to move more efficiently on soft soil,  
925 enhancing the surface area of the pes and preventing it from sinking into mud. In our view, having  
926 robust bones should be viewed as an allometric consequence of a shortening of the limb in those  
927 species, this shortening being either related to a semi-aquatic lifestyle or/and to an adaptation for  
928 grazing. As the precise lifestyle of short-legged rhinos is still debated nowadays, further  
929 investigations on these brachypodial taxa should help to clarify the origin and functional roles of this  
930 particular condition.

### 931 **Differences within and between fore- and hind limb bones**

932 Comparison with data obtained for forelimb bones (Mallet *et al.*, in press) clearly underlines that the  
933 stylopodial elements of the fore- and hind limbs share similar patterns of shape variation. The  
934 morphological changes of both the humerus and femur appear simultaneously correlated with size,  
935 mass and gracility index while also carrying a strong phylogenetic signal. Toward high body mass,  
936 both humerus and femur display an increase of the general robustness, associated with a  
937 development of both epiphyses, the reinforcement of muscular insertions (mainly for extensors and  
938 flexors) and their displacement leading to lengthened lever arms. At the opposite, zeugopodial  
939 elements are mainly impacted by the degree of brachypody (at the scale of the whole superfamily),  
940 related to the distribution of the mass within the body rather to the absolute mass itself.



941 Furthermore, the shape of radius and tibia, both supporting directly the body weight, are more  
942 related to mass than ulna and fibula shapes. Highly brachypodial taxa display an increase of  
943 robustness and a broadening of the epiphyses as well. Some anatomical areas, like the medial and  
944 lateral parts of the proximal epiphysis of both the radius and tibia, show a remarkably similar trend  
945 of shape variation towards a high degree of brachypody. All these results partially invalidate the fifth  
946 hypothesis, as differences in patterns of shape variation are stronger between the stylopodium and  
947 zeugopodium than between the fore- and hind limbs. Similar observations were partially obtained on  
948 modern rhinos (Mallet *et al.*, 2019, 2020) and this general trend may indicate that serial homology  
949 between fore- and hind limb elements remain strong (Young & Hallgrímsson, 2005) despite different  
950 functional requirements (Henderson, 1999; Regnault *et al.*, 2013; Panagiotopoulou *et al.*, 2019).

951 However, some differences in functional role do exist between fore- and hind limbs. While body  
952 mass was correlated with the gracility index (GI-MC3 computed on the third metacarpal) in the  
953 forelimb bones (Mallet *et al.*, in press), this correlation is not significant with GI-MT3. Yet the  
954 distribution of these two indices remains extremely similar, possessing same means and variance  
955 (see Supplementary Figure S5). In other words, the variation in gracility index of the hind limb is  
956 decoupled from that of body mass, while they are more closely associated for the forelimb. This  
957 highlights differences of general organisation between fore- and hind limbs and supports the idea  
958 that forelimb bones among Rhinoceroidea may be more constrained by the weight repartition than  
959 are the hind limb ones, in association with their involvement in other functions like ensuring a  
960 powerful propulsion (Heglund *et al.*, 1982; Alexander, 1985; Dutton *et al.*, 2006; Henderson, 2006;  
961 Regnault *et al.*, 2013; Panagiotopoulou *et al.*, 2019) (Fig. 12).

962 Moreover, the bones constituting the elbow and knee joints might show a modular organisation (the  
963 modular condition of the tibia remaining to be tested as well). In the forelimb, the trends in shape  
964 variation were similar between the complete humerus and its distal part, which displayed similarities  
965 with the proximal ulna (such as a significant correlation with CS, BM and GI simultaneously).

966 Conversely, on the hind limb, the shape variation of the complete femur is only congruent with that  
967 of its proximal part, while that of its distal part is more congruent with that of the tibia.

968 Consequently, if morphological modules exist in the elbow and the knee joints of Rhinoceroidea,  
969 they may not be organised in a homologous way, the former involving the entire humerus and the  
970 proximal ulna while the latter would involve only the distal femur and the entire tibia. These  
971 differences, which will require further testing, may be related to the distinct joint construction  
972 between the fore- and hind limb. Beyond their respective bending in opposite directions, the elbow  
973 joint constitutes a strongly constrained hinge restricted to craniocaudal movements only, formed by  
974 the humerus, the radius and the ulna together. Conversely, the knee joint allows slight mediolateral

975 rotations in addition to craniocaudal movements (Hildebrand, 1974), although reduced by the  
976 passive stay apparatus. Moreover, the knee joint also differs from the elbow in involving a sesamoid  
977 bone, the patella, and should be considered as functionally homologous to the shoulder region  
978 (Schmidt & Fischer, 2009). This difference of configuration in those two joints may therefore involve  
979 differences in shape patterns of the bones constituting them. Only a larger investigation of potential  
980 morphological modules and on the construction of these joints could shed light on these questions.

#### 981 **Graviportality: an irrelevant concept in rhinocerotoids?**

982 Finally, the addition of the results on hind limb (this study) to those obtained on forelimb (Mallet *et*  
983 *al.*, in press) enables the critical evaluation of the concept of graviportality and its application to  
984 Rhinoceroidea (Hutchinson, 2021). The shape of the limb bones in Rhinoceroidea diversified  
985 broadly during the more than 50 Ma of evolution of this group, while its variation still carries a strong  
986 phylogenetic signal. Yet, the general construction of the rhino limbs largely follows a similar pattern  
987 across all the superfamily; this “rhinocerotoid” general pattern being easily distinguishable from  
988 those of close relative (e.g., horses, tapirs) and of other heavy mammals (e.g., proboscideans).  
989 Convergences towards a high body mass are observed in close clades within Perissodactyla (e.g.,  
990 Lophiodontidae and Brontotherioidea exceeding 2,000 kg [Damuth & MacFadden, 1990; Robinet *et*  
991 *al.*, 2015], Chalicotherioidea exceeding 1,500 kg – [Guérin, 2012]) and in related groups among  
992 “panperissodactyls” (Welker *et al.*, 2015) such as South American native ungulates (Notoungulata  
993 and Litopterna, sometimes exceeding a ton – MacFadden, 2005; Farina, Czerwonogora, & Giacomo,  
994 2014). Yet, all these heavy ungulates have unique morphologies that share few morphological  
995 resemblances with Rhinoceroidea.

996 As detailed previously (see Introduction), Gregory (1912) and Osborn (1929) defined graviportal  
997 animals by having relatively long stylopodium and short autopodium, body mass of several hundreds  
998 of kilograms, columnar limbs, large and strong bones, large feet, slow pace. When considering this  
999 morphofunctional framework and these criteria classically associated with graviportality, no deep  
1000 architectural breakdown towards this peculiar limb organisation has been observed in rhinos. The  
1001 high body mass and the increase in bone robustness, associated with enlarged feet (although this  
1002 criterion is relative; Panagiotopoulou, Pataky & Hutchinson, 2019), are almost the only graviportal  
1003 features encountered in the superfamily. The morphology of the elbow and knee joints indicate that  
1004 almost all taxa in Rhinoceroidea retain flexed limbs (as in most small and large ungulates in  
1005 general) with no convergence towards a strictly columnar organisation. Only large Paraceratheriidae  
1006 display straighter limbs, although they are not totally columnar (elbow and knee joints likely  
1007 remaining flexed, rather reminiscent of the giraffid sivatheres for example) (Fortelius & Kappelman,

1008 1993; Paul, 1997; Paul & Christiansen, 2000). The relative lengthening of the stylopodium relatively  
1009 to the other limb elements is far from being clear except in highly brachypodial species (but more  
1010 likely due to a shortening of the zeugopodium). The reduction of the autopodium elements (i.e.,  
1011 degree of brachypody) appears associated with various body mass values and not only the highest  
1012 ones. Conversely, the reduction of the autopodium is not always marked in heavy taxa, as observed  
1013 in *Elasmotherium* and *Paraceratherium* (Mallet *et al.*, in press). Although not directly studied here,  
1014 the gait of rhinos seems also relatively conservative: modern rhinos are able to gallop (Alexander &  
1015 Pond, 1992) and given the similar general construction of the limbs in large fossil taxa, it is likely that  
1016 most of them could reach a relatively fast pace (Paul & Christiansen, 2000).

1017 Conversely, our detailed study of limb long bones in rhinos highlights the morphological changes  
1018 undergone by the zeugopodium as rhinocerotoids increased in mass, although this aspect was nearly  
1019 absent from the classical framework of graviportality. The shape changes observed in the  
1020 zeugopodial elements relative to the degree of brachypody (and, consequently, to the vertical height  
1021 of the centre of gravity) shed light on the impact of mass distribution on this segment. While the  
1022 works of Gregory and Osborn assumed that the relative length of this central segment is poorly  
1023 modified between cursorial and graviportal taxa (Gregory, 1912; Osborn, 1929), results obtained on  
1024 rhinocerotoids highlight that the zeugopodium shape is on the contrary deeply modified between  
1025 light and heavy rhinos.

1026 Among heavy taxa, Paraceratheriidae challenge the classic definition of graviportality even more  
1027 than other rhinos (Granger & Gregory, 1936; Fortelius & Kappelman, 1993). Particularly, they do not  
1028 show the relative reduction of the autopodium length or the fully columnar limbs expected for such  
1029 big quadrupeds. Moreover, the ratio “humeral length over radial length” is below 1 in *Juxia* and  
1030 *Urtinotherium* (Paraceratheriidae) while above 1 for the small runner *Hyracodon* (Hyracodontidae),  
1031 making Paraceratheriidae close to more gracile, specialized cursors such as modern equids (ratio < 1).  
1032 This ratio is also different from that observed in other rhinos (e.g., > 1 for modern rhinos).

1033 Conversely, the ratio “femoral length over tibial length” is higher in *Paraceratherium* (1.4) than in  
1034 *Hyrachyus* (1.1) and modern horses (1.1). This ratio on the hind limb is close to that observed in  
1035 modern rhinos (1.5 in *C. simum*, 1.4 in *Dc. bicornis*) (C.M. personal computations). These ratios  
1036 coupled with our results show that Paraceratheriidae appear to follow a different trend of limb  
1037 architecture than the rest of the superfamily. Unlike in other Rhinoceroidea, the shape of their  
1038 stylopodium is highly derived relatively to more basal rhinocerotoids, while that of their  
1039 zeugopodium is poorly modified and retains a plesiomorphic aspect (although relatively more robust)  
1040 close to that of small taxa like Hyrachyidae and Hyracodontidae (Mallet *et al.*, in press). This  
1041 conservative shape of the zeugopodium in paraceratheres is more marked on the forelimb than on

1042 the hind limb, which would appear in contradiction with the forelimb supporting a higher part of the  
1043 total weight. This atypical pattern of shape variation could be related to the long neck and heavy  
1044 head borne by paraceratheriids (P.-O. Antoine, pers. comm.), as well as to the slightly sloped  
1045 backbone (Prothero, 2005), two uncommon features among Rhinoceroidea which mostly display a  
1046 short neck and a relatively horizontal spine (Paul & Christiansen, 2000; Qiu & Wang, 2007; Prothero,  
1047 2013). It is also possible that the forelimb of Paraceratheriidae hardly follows the general trend  
1048 common to most Rhinoceroidea, due to strong developmental or evolutionary constraints. All  
1049 these features highlight morphological features linked to both high body mass support (e.g.,  
1050 robustness of the stylopodium, shortening of the tibia) and the persistence of a cursorial  
1051 construction close to that of small Hyrachyidae and Hyracodontidae. This unusual architecture  
1052 tackles the classical opposition between “cursorial” and “graviportal” categories, Paraceratheriidae  
1053 appearing to show features characterizing both categories simultaneously.

1054 As Rhinoceroidea hardly display the anatomical criteria classically associated with graviportal  
1055 two possible assessments arise: either Rhinoceroidea should not be considered graviportal, or the  
1056 graviportal framework is too limited to describe the diverse conditions by which species adapt to  
1057 heavy weight (Hutchinson, 2021). The limitations of the framework of Gregory (1912) and Osborn  
1058 (1929) may be related to the archetypal groups used to define graviportal (and cursoriality), as  
1059 they mainly considered elephants and extinct groups with a similar limb architecture like Dinocera  
1060 in this regard (Osborn, 1900). However, it is not sure that all anatomical features originally defined as  
1061 graviportal in these groups are in fact linked to a high body mass and are shared by all heavy  
1062 quadrupedal taxa. Most Proboscidea retain poorly modified limbs, with no reduction of the digit  
1063 number, no radio-ulnar and tibio-fibular fusion (two traits that are, however, found in  
1064 Rhinoceroidea), a symmetrical femoral trochlea. Their ulna directly supports the humerus in the  
1065 elbow joint, contrary to the condition in most ungulates, where the humerus is supported almost  
1066 only by the radius (Fujiwara, 2009; Janis *et al.*, 2012; Larramendi, 2016). Morphofunctional  
1067 investigations highlight that the limb structure and motion in Proboscidea is atypical compared to  
1068 that in most mammalian quadrupeds, including heavy ones (Ren *et al.*, 2010). Except in their general  
1069 increase of robustness, Rhinoceroidea show no clear convergence of shape or limb construction  
1070 with that of Proboscidea, especially in extremely large but gracile taxa like Paraceratheriidae. Most  
1071 criteria associated with graviportal in elephants are thus not universally shared in heavy  
1072 quadrupeds showing that the classic graviportal framework should be considered with caution  
1073 (Hutchinson, 2021). Therefore, it may be more relevant to search for the features repeatedly  
1074 encountered in diverse taxa showing a high body mass before defining a general concept such as  
1075 graviportal. As sustaining a heavy weight likely involves a mosaic of traits, graviportal should

1076 only be used after deciphering the repeated features potentially associated to it and the special  
1077 adaptations limited to each particular group. Taking into account the locomotor behaviour of a given  
1078 animal should also help to refine the concepts of “graviportality” and “cursoriality”.

1079 **CONCLUSION**

1080 Beyond a common increase of robustness and reinforcement of muscular insertions towards higher  
1081 body mass, the shape of stylopodial and zeugopodial bones among Rhinoceroidea does not follow  
1082 the same pattern of variation. More morphological differences are also observed between the  
1083 stylopodium and zeugopodium than between fore- and hind limbs. Rather than the overall absolute  
1084 body mass, the distribution of mass within the body and the position of the centre of gravity, linked  
1085 to the degree of brachypody, that seems to drive the shape variation of hind limb bones. Conversely,  
1086 only the fibula exhibits a puzzling relationship between shape and body proportions. Our results also  
1087 highlight the potential modularity of the femur, with a distal region varying in shape in similar ways  
1088 to the tibia and fibula. Together with our previous results on the forelimb, this points out the need to  
1089 explore shape patterns beyond the units constituted by single bones. Finally, the integrative  
1090 investigation of limb bones among Rhinoceroidea underlines the limits of the concept of  
1091 graviportality to describe the morphology of these animals. It calls for a refining of this century-old  
1092 framework, considering the anatomical specificities of each group displaying an increase of body  
1093 mass through time.

1094

1095 **ACKNOWLEDGMENTS**

1096 The authors would like to warmly thank all the curators of the visited institutions for granting us  
1097 access to the studied specimens: E. Hoeger, S. Ketelsen, R. O’Leary and J. Meng (American Museum  
1098 of Natural History, New York, USA), J.-M. Pouillon and C. Bouix (Association Rhinopolis, Gannat,  
1099 France), G. Rößner (Bayerische Staatssammlung für Paläontologie und Geologie, Munich, Germany),  
1100 D. Berthet (Centre de Conservation et d’Étude des Collections, Musée des Confluences, Lyon,  
1101 France), E. Robert (Collections de Géologie de Lyon, Université Lyon 1 Claude Bernard, Lyon, France),  
1102 Yves Laurent (Muséum d’Histoire Naturelle de Toulouse, Toulouse, France), J. Lesur, A. Verguin  
1103 (Muséum National d’Histoire Naturelle, Paris, France), R. Portela-Miguez, P. Brewer and R. Pappa  
1104 (Natural History Museum, London, UK), L. Costeur and F. Dammeyer (Naturhistorisches Museum  
1105 Basel, Basel, Switzerland), A. Folie, C. Cousin, O. Pauwels and S. Bruaux (Royal Belgian Institute of  
1106 Natural Sciences, Brussels, Belgium), E. Gilissen (Royal Museum for Central Africa, Tervuren, Belgium)  
1107 and D. Brinkman (Yale Peabody Museum, New Haven, CT, USA). We would also like to thanks M. C.  
1108 Reyes from the National Museum of the Philippines (Manila, Philippines) and T. Ingicco from the  
1109 MNHN (Paris, France) for providing the 3D models of *N. philippinensis*, and J. Hutchinson from the  
1110 Royal Veterinary College (London, UK) for providing us CT-scan data coming from the University of  
1111 California Museum of Paleontology (Berkeley, USA). We are grateful to S. Castiglione and P. Raia  
1112 (University of Naples Federico II, Naples, Italy) for their precious help in using the RRphylo package.  
1113 We warmly thanks P.-O. Antoine and one anonymous reviewer for their positive and constructive  
1114 comments allowing us to greatly improve the final quality of this work. Many thanks to K. Gaignebet  
1115 and C. Bouquet for their help in reconstructing many 3D models. C.M. acknowledges C. Etienne, R.  
1116 Lefebvre and R. Pintore (MNHN, Paris, France) for constructive discussions and advices on R  
1117 programming, data analyses and interpretations. This work was funded by the European Research  
1118 Council and is part of the GRAVIBONE project (ERC-2016-STG-715300).

1119 **AUTHOR CONTRIBUTIONS**

1120 C.M. designed the study with significant inputs from A.H., R.C. and G.B. C.M. did the data acquisition  
1121 with inputs from A.H. C.M. performed the analyses with the help of R.C and G.B. and all authors  
1122 interpreted the results. C.M. drafted the manuscript. All authors reviewed and contributed to the  
1123 final version of the manuscript, read it and approved it.

1124 **DATA AVAILABILITY**

1125 The data underlying this article will be shared on reasonable request to the corresponding author.  
1126 Most of the 3D models will be or have been deposited on the 3D online repository MorphoSource at  
1127 the following address: <https://www.morphosource.org/projects/000366286?locale=en>.



1128 **REFERENCES**

- 1129 3D Systems Corporation. 2014. *Geomagic Studio*. 3D Systems Corporation.
- 1130 Adams DC. 2014. A generalized K statistic for estimating phylogenetic signal from shape and  
1131 other high-dimensional multivariate data. *Systematic Biology* 63: 685–697.
- 1132 Adams DC, Collyer ML. 2018. Multivariate Phylogenetic Comparative Methods: Evaluations,  
1133 Comparisons, and Recommendations. *Systematic Biology* 67: 14–31.
- 1134 Adams DC, Otárola-Castillo E. 2013. geomorph: an r package for the collection and analysis  
1135 of geometric morphometric shape data. *Methods in Ecology and Evolution* 4: 393–399.
- 1136 Adams DC, Rohlf FJ, Slice DE. 2004. Geometric morphometrics: Ten years of progress  
1137 following the ‘revolution’. *Italian Journal of Zoology* 71: 5–16.
- 1138 Agisoft. 2018. *PhotoScan Professional Edition*. Agisoft.
- 1139 Alexander RM. 1985. Mechanics of posture and gait of some large dinosaurs. *Zoological*  
1140 *Journal of the Linnean Society* 83: 1–25.
- 1141 Alexander RM, Pond CM. 1992. Locomotion and bone strength of the white rhinoceros,  
1142 *Ceratotherium simum*. *Journal of Zoology* 227: 63–69.
- 1143 Antoine PO. 2002. Phylogénie et évolution des Elasmotheriina (Mammalia, Rhinocerotidae).  
1144 *Mémoires du Muséum National d’Histoire Naturelle (1993)* 188: 5–350.
- 1145 Antoine PO, Downing KF, Crochet JY, Duranthon F, Flynn LJ, Marivaux L, Métais G, Rajpar AR,  
1146 Roohi G. 2010. A revision of *Aceratherium blanfordi* Lydekker, 1884 (Mammalia:  
1147 Rhinocerotidae) from the Early Miocene of Pakistan: postcranials as a key. *Zoological Journal*  
1148 *of the Linnean Society* 160: 139–194.
- 1149 Antoine PO, Duranthon F, Welcomme JL. 2003. *Alicornops* (Mammalia, Rhinocerotidae) dans  
1150 le Miocène supérieur des Collines Bugti (Balouchistan, Pakistan): implications  
1151 phylogénétiques. *Geodiversitas* 25: 575–603.
- 1152 Antoine PO, Reyes MC, Amano N, Bautista AP, Chang CH, Claude J, De Vos J, Ingicco T. 2021.  
1153 A new rhinoceros clade from the Pleistocene of Asia sheds light on mammal dispersals to the  
1154 Philippines. *Zoological Journal of the Linnean Society*.
- 1155 Arambourg C. 1959. Vertébrés continentaux du Miocène supérieur de l’Afrique du Nord.  
1156 *Publications du Service de la Carte Géologique de l’Algérie (Nouvelle Série), Paléontologie,*  
1157 *Mémoire, Serv. de la Carte Géol. de l’Algérie* 4: 1–161.
- 1158 Artec 3D. 2018. *Artec Studio Professional*. Artec 3D.
- 1159 Averianov A, Danilov I, Jin J, Wang Y. 2017. A new amynodontid from the Eocene of South  
1160 China and phylogeny of Amynodontidae (Perissodactyla: Rhinocerotidae). *Journal of*  
1161 *Systematic Palaeontology* 15: 927–945.

- 1162 Bai B, Meng J, Wang YQ, Wang HB, Holbrook L. 2017. Osteology of The Middle Eocene  
1163 Ceratomorph *Hyrachyus modestus* (Mammalia, Perissodactyla). *Bulletin of the American*  
1164 *Museum of Natural History*: 1–70.
- 1165 Bai B, Meng J, Zhang C, Gong YX, Wang YQ. 2020. The origin of Rhinocerotoida and  
1166 phylogeny of Ceratomorpha (Mammalia, Perissodactyla). *Communications Biology* 3: 1–16.
- 1167 Baker J, Meade A, Pagel M, Venditti C. 2015. Adaptive evolution toward larger size in  
1168 mammals. *Proceedings of the National Academy of Sciences* 112: 5093–5098.
- 1169 Bardua C, Felice RN, Watanabe A, Fabre AC, Goswami A. 2019. A Practical Guide to Sliding  
1170 and Surface Semilandmarks in Morphometric Analyses. *Integrative Organismal Biology* 1: 1–  
1171 34.
- 1172 Barone R. 2010a. *Anatomie comparée des mammifères domestiques. Tome 1 : Ostéologie*.  
1173 Paris: Vigot Frères.
- 1174 Barone R. 2010b. *Anatomie comparée des mammifères domestiques. Tome 2 : Arthrologie et*  
1175 *myologie*. Paris: Vigot Frères.
- 1176 Baylac M, Frieß M. 2005. Fourier Descriptors, Procrustes Superimposition, and Data  
1177 Dimensionality: An Example of Cranial Shape Analysis in Modern Human Populations. In:  
1178 Slice DE, ed. *Developments in Primatology: Progress and Prospects. Modern Morphometrics*  
1179 *in Physical Anthropology*. Boston, MA: Springer US, 145–165.
- 1180 Becker D. 2003. Paléoécologie et paléoclimats de la molasse du Jura (oligo-miocène).  
1181 Unpublished thesis, Université de Fribourg.
- 1182 Becker D, Antoine PO, Maridet O. 2013. A new genus of Rhinocerotidae (Mammalia,  
1183 Perissodactyla) from the Oligocene of Europe. *Journal of Systematic Palaeontology* 11: 947–  
1184 972.
- 1185 Becker D, Bürgin T, Oberli U, Scherler L. 2009. *Diaceratherium lemanense* (Rhinocerotidae)  
1186 from Eschenbach (eastern Switzerland): systematics, palaeoecology, palaeobiogeography.  
1187 *Neues Jahrbuch für Geologie und Paläontologie-Abhandlungen* 254: 5–39.
- 1188 Bertram JEA, Biewener AA. 1990. Differential scaling of the long bones in the terrestrial  
1189 carnivora and other mammals. *Journal of Morphology* 204: 157–169.
- 1190 Biasatti D, Wang Y, Deng T. 2018. Paleoecology of Cenozoic rhinos from northwest China: a  
1191 stable isotope perspective. *Vertebrata Palasiatica* 56: 45–68.
- 1192 Biewener AA. 1989a. Mammalian Terrestrial Locomotion and Size. *BioScience* 39: 776–783.
- 1193 Biewener AA. 1989b. Scaling body support in mammals: limb posture and muscle mechanics.  
1194 *Science* 245: 45–48.
- 1195 Biewener AA, Patek SN. 2018. *Animal Locomotion*. New York: Oxford University Press.

- 1196 Billet G, Bardin J. 2021. Segmental Series and Size: Clade-Wide Investigation of Molar  
1197 Proportions Reveals a Major Evolutionary Allometry in the Dentition of Placental Mammals.  
1198 *Systematic Biology*.
- 1199 Blomberg SP, Garland T, Ives AR, Crespi B. 2003. Testing for phylogenetic signal in  
1200 comparative data: behavioral traits are more labile. *Evolution* 57: 717–745.
- 1201 Boada-Saña A. 2008. Phylogénie du rhinocérotidé *Diaceratherium* Dietrich, 1931 (Mammalia,  
1202 Perissodactyla).
- 1203 Boada-Saña A, Hervet S, Antoine PO. 2007. Nouvelles données sur les rhinocéros fossiles de  
1204 Gannat (Allier, limite Oligocène-Miocène). *Revue des Sciences Naturelles d’Auvergne* 71: 3–  
1205 25.
- 1206 Bokma F, Godinot M, Maridet O, Ladevèze S, Costeur L, Solé F, Gheerbrant E, Peigné S,  
1207 Jacques F, Laurin M. 2016. Testing for Depéret’s Rule (Body Size Increase) in Mammals using  
1208 Combined Extinct and Extant Data. *Systematic Biology* 65: 98–108.
- 1209 Botton-Divet L, Cornette R, Fabre AC, Herrel A, Houssaye A. 2016. Morphological Analysis of  
1210 Long Bones in Semi-aquatic Mustelids and their Terrestrial Relatives. *Integrative and*  
1211 *Comparative Biology* 56: 1298–1309.
- 1212 Botton-Divet L, Cornette R, Houssaye A, Fabre AC, Herrel A. 2017. Swimming and running: a  
1213 study of the convergence in long bone morphology among semi-aquatic mustelids  
1214 (Carnivora: Mustelidae). *Biological Journal of the Linnean Society* 121: 38–49.
- 1215 Cappellini E, Welker F, Pandolfi L, Ramos-Madriral J, Samodova D, Rüter PL, Fotakis AK,  
1216 Lyon D, Moreno-Mayar JV, Bukhsianidze M, Jersie-Christensen RR, Mackie M, Ginolhac A,  
1217 Ferring R, Tappen M, Palkopoulou E, Dickinson MR, Stafford TW, Chan YL, Götherström A,  
1218 Nathan SKSS, Heintzman PD, Kapp JD, Kirillova I, Moodley Y, Agusti J, Kahlke RD, Kiladze G,  
1219 Martínez-Navarro B, Liu S, Velasco MS, Sinding MHS, Kelstrup CD, Allentoft ME, Orlando L,  
1220 Penkman K, Shapiro B, Rook L, Dalén L, Gilbert MTP, Olsen JV, Lordkipanidze D, Willerslev E.  
1221 2019. Early Pleistocene enamel proteome from Dmanisi resolves *Stephanorhinus* phylogeny.  
1222 *Nature* 574: 103–107.
- 1223 Carrano MT. 1999. What, if anything, is a cursor? Categories versus continua for determining  
1224 locomotor habit in mammals and dinosaurs. *Journal of Zoology* 247: 29–42.
- 1225 Cassini GH, Vizcaíno SF, Bargo MS. 2012. Body mass estimation in Early Miocene native  
1226 South American ungulates: a predictive equation based on 3D landmarks. *Journal of Zoology*  
1227 287: 53–64.
- 1228 Castiglione S, Tesone G, Piccolo M, Melchionna M, Mondanaro A, Serio C, Febbraro MD, Raia  
1229 P. 2018. A new method for testing evolutionary rate variation and shifts in phenotypic  
1230 evolution. *Methods in Ecology and Evolution* 9: 974–983.
- 1231 Cerdeño E. 1995. Cladistic analysis of the family Rhinocerotidae (Perissodactyla). *American*  
1232 *Museum novitates* 3143: 1–25.

- 1233 Cerdeño E. 1998. Diversity and evolutionary trends of the Family Rhinocerotidae  
1234 (Perissodactyla). *Palaeogeography, Palaeoclimatology, Palaeoecology* 141: 13–34.
- 1235 Chen S, Deng T, Hou S, Shi Q, Pang L. 2010. Sexual Dimorphism in Perissodactyl Rhinocerotid  
1236 *Chilotherium wimani* from the Late Miocene of the Linxia Basin (Gansu, China). *Acta*  
1237 *Palaeontologica Polonica* 55: 587–597.
- 1238 Cignoni P, Callieri M, Corsini M, Dellepiane M, Ganovelli F, Ranzuglia G. 2008. *MeshLab: an*  
1239 *Open-Source Mesh Processing Tool*. The Eurographics Association.
- 1240 Clementz MT, Holroyd PA, Koch PL. 2008. Identifying Aquatic Habits Of Herbivorous  
1241 Mammals Through Stable Isotope Analysis. *Palaaios* 23: 574–585.
- 1242 Colbert EH. 1938. Fossil mammals from Burma in the American Museum of Natural History.  
1243 *Bulletin of the American Museum of Natural History* 74: 255–436.
- 1244 Coombs WP. 1978. Theoretical Aspects of Cursorial Adaptations in Dinosaurs. *The Quarterly*  
1245 *Review of Biology* 53: 393–418.
- 1246 Cope ED. 1887. *The origin of the fittest: Essays on evolution*. New York: Appleton.
- 1247 Crelin ES. 1988. Ligament of the head of the femur in the orangutan and Indian elephant.  
1248 *The Yale Journal of Biology and Medicine* 61: 383–388.
- 1249 Damuth JD, MacFadden BJ. 1990. *Body Size in Mammalian Paleobiology: Estimation and*  
1250 *Biological Implications*. Cambridge University Press.
- 1251 Depéret C. 1907. *Les transformations du monde animal*. Paris: Flammarion.
- 1252 Dinerstein E. 1991. Sexual Dimorphism in the Greater One-Horned Rhinoceros (*Rhinoceros*  
1253 *unicornis*). *Journal of Mammalogy* 72: 450–457.
- 1254 Dinerstein E. 2011. Family Rhinocerotidae (Rhinoceroses). In: Wilson DE, Mittermeier RA,  
1255 eds. *Handbook of the Mammals of the World*. Barcelona: Don E. Wilson & Russel A.  
1256 Mittermeier, 144–181.
- 1257 Dutto DJ, Hoyt DF, Clayton HM, Cogger EA, Wickler SJ. 2006. Joint work and power for both  
1258 the forelimb and hindlimb during trotting in the horse. *Journal of Experimental Biology* 209:  
1259 3990–3999.
- 1260 Eisenmann V, Guérin C. 1984. Morphologie fonctionnelle et environnement chez les  
1261 périssodactyles. *Geobios* 17: 69–74.
- 1262 Ercoli MD, Prevosti FJ. 2011. Estimación de Masa de las Especies de Sparassodonta  
1263 (Mammalia, Metatheria) de Edad Santacrucesense (Mioceno Temprano) a Partir del Tamaño  
1264 del Centroides de los Elementos Apendiculares: Inferencias Paleoecológicas. *Ameghiniana* 48:  
1265 462–479.

- 1266 Etienne C, Filippo A, Cornette R, Houssaye A. 2020a. Effect of mass and habitat on the shape  
1267 of limb long bones: A morpho-functional investigation on Bovidae (Mammalia:  
1268 Cetartiodactyla). *Journal of Anatomy* 238: 886–904.
- 1269 Etienne C, Houssaye A, Hutchinson JR. 2021. Limb myology and muscle architecture of the  
1270 Indian rhinoceros *Rhinoceros unicornis* and the white rhinoceros *Ceratotherium simum*  
1271 (Mammalia: Rhinocerotidae). *PeerJ* 9: e11314.
- 1272 Etienne C, Mallet C, Cornette R, Houssaye A. 2020b. Influence of mass on tarsus shape  
1273 variation: a morphometrical investigation among Rhinocerotidae (Mammalia:  
1274 Perissodactyla). *Biological Journal of the Linnean Society* 129: 950–974.
- 1275 Farina RA, Czerwonogora A, Giacomo MD. 2014. Splendid oddness: revisiting the curious  
1276 trophic relationships of South American Pleistocene mammals and their abundance. *Anais*  
1277 *da Academia Brasileira de Ciências* 86: 311–331.
- 1278 Fau M, Cornette R, Houssaye A. 2016. Photogrammetry for 3D digitizing bones of mounted  
1279 skeletons: Potential and limits. *Comptes Rendus Palevol* 15: 968–977.
- 1280 Federative Committee on Anatomical Terminology. 1998. *Terminologia Anatomica*. Georg  
1281 Thieme Verlag.
- 1282 Felsenstein J. 1985. Phylogenies and the Comparative Method. *The American Naturalist* 125:  
1283 1–15.
- 1284 Felsenstein J. 2004. *Inferring Phylogenies*. Sunderland, Mass: OUP USA.
- 1285 Fernando P, Polet G, Foad N, Ng LS, Pastorini J, Melnick DJ. 2006. Genetic diversity,  
1286 phylogeny and conservation of the Javan rhinoceros (*Rhinoceros sondaicus*). *Conservation*  
1287 *Genetics* 7: 439–448.
- 1288 Fischer MS, Blickhan R. 2006. The tri-segmented limbs of therian mammals: kinematics,  
1289 dynamics, and self-stabilization—a review. *Journal of Experimental Zoology Part A:*  
1290 *Comparative Experimental Biology* 305A: 935–952.
- 1291 Fisher RE, Scott KM, Adrian B. 2010. Hind limb myology of the common hippopotamus,  
1292 *Hippopotamus amphibius* (Artiodactyla: Hippopotamidae). *Zoological Journal of the Linnean*  
1293 *Society* 158: 661–682.
- 1294 Fortelius M, Kappelman J. 1993. The largest land mammal ever imagined. *Zoological Journal*  
1295 *of the Linnean Society* 108: 85–101.
- 1296 Fujiwara S ichi. 2009. Olecranon orientation as an indicator of elbow joint angle in the stance  
1297 phase, and estimation of forelimb posture in extinct quadruped animals. *Journal of*  
1298 *Morphology* 270: 1107–1121.
- 1299 Gaudry M. 2017. Molecular phylogenetics of the rhinoceros clade and evolution of UCP1  
1300 transcriptional regulatory elements across the mammalian phylogeny. Unpublished thesis,  
1301 University of Manitoba.

- 1302 Goolsby EW. 2015. Phylogenetic Comparative Methods for Evaluating the Evolutionary  
1303 History of Function-Valued Traits. *Systematic Biology* 64: 568–578.
- 1304 Goswami A, Polly PD. 2010. Methods for Studying Morphological Integration and Modularity.  
1305 *The Paleontological Society Papers* 16: 213–243.
- 1306 Gower JC. 1975. Generalized procrustes analysis. *Psychometrika* 40: 33–51.
- 1307 Granger W, Gregory WK. 1936. Further notes on the gigantic extinct rhinoceros,  
1308 *Baluchitherium*, from the Oligocene of Mongolia. *Bulletin of the American Museum of*  
1309 *Natural History* 72: 1–73.
- 1310 Gregory WK. 1912. Notes on the Principles of Quadrupedal Locomotion and on the  
1311 Mechanism of the Limbs in Hoofed Animals. *Annals of the New York Academy of Sciences* 22:  
1312 267–294.
- 1313 Guérin C. 1980. Les Rhinocéros (Mammalia, Perissodactyla) du Miocène terminal au  
1314 Pléistocène supérieur en Europe occidentale. Comparaison avec les espèces actuelles.
- 1315 Guérin C. 1989. La famille des Rhinocerotidae (Mammalia, Perissodactyla) : systématique,  
1316 histoire, évolution, paléoécologie. *Cranium* 6: 3–14.
- 1317 Guérin C. 2012. Anisodon grande (Perissodactyla, Chalicotheriidae) de Sansan. *Mémoires du*  
1318 *Muséum national d'histoire naturelle. Mammifères de Sansan*. Paris, 279–315.
- 1319 Gunz P, Mitteroecker P. 2013. Semilandmarks: a method for quantifying curves and surfaces.  
1320 *Hystrix, the Italian Journal of Mammalogy* 24: 103–109.
- 1321 Gunz P, Mitteroecker P, Bookstein FL. 2005. Semilandmarks in Three Dimensions. In: Slice  
1322 DE, ed. *Developments in Primatology: Progress and Prospects. Modern Morphometrics in*  
1323 *Physical Anthropology*. Boston, MA: Slice, D. E., 73–98.
- 1324 Hallgrímsson B, Katz DC, Aponte JD, Larson JR, Devine J, Gonzalez PN, Young NM, Roseman  
1325 CC, Marcucio RS. 2019. Integration and the Developmental Genetics of Allometry.  
1326 *Integrative and Comparative Biology* 59: 1369–1381.
- 1327 Hallgrímsson B, Willmore K, Hall BK. 2002. Canalization, developmental stability, and  
1328 morphological integration in primate limbs. *American Journal of Physical Anthropology* 119:  
1329 131–158.
- 1330 Hanot P, Herrel A, Guintard C, Cornette R. 2017. Morphological integration in the  
1331 appendicular skeleton of two domestic taxa: the horse and donkey. *Proc. R. Soc. B* 284:  
1332 20171241.
- 1333 Heglund NC, Cavagna GA, Taylor CR. 1982. Energetics and mechanics of terrestrial  
1334 locomotion. III. Energy changes of the centre of mass as a function of speed and body size in  
1335 birds and mammals. *Journal of Experimental Biology* 97: 41–56.
- 1336 Heissig K. 2012. Les Rhinocerotidae (Perissodactyla) de Sansan. In: Peigné S, Sen S, eds.  
1337 *Mémoires du Muséum national d'histoire naturelle. Mammifères de Sansan*. Paris, 317–485.

- 1338 Henderson DM. 1999. Estimating the Masses and Centers of Mass of Extinct Animals by 3-D  
1339 Mathematical Slicing. *Paleobiology* 25: 88–106.
- 1340 Henderson DM. 2006. Burly gaits: centers of mass, stability, and the trackways of sauropod  
1341 dinosaurs. *Journal of Vertebrate Paleontology* 26: 907–921.
- 1342 Hermanson JW, MacFadden BJ. 1992. Evolutionary and functional morphology of the  
1343 shoulder region and stay-apparatus in fossil and extant horses (Equidae). *Journal of*  
1344 *Vertebrate Paleontology* 12: 377–386.
- 1345 Hermanson JW, MacFadden BJ. 1996. Evolutionary and functional morphology of the knee in  
1346 fossil and extant horses (Equidae). *Journal of Vertebrate Paleontology* 16: 349–357.
- 1347 Hildebrand M. 1974. *Analysis of vertebrate structure*. New York: John Wiley & Sons.
- 1348 Ho J, Tumkaya T, Aryal S, Choi H, Claridge-Chang A. 2019. Moving beyond P values: data  
1349 analysis with estimation graphics. *Nature Methods* 16: 565–566.
- 1350 Houssaye A, Fernandez V, Billet G. 2016. Hyperspecialization in Some South American  
1351 Endemic Ungulates Revealed by Long Bone Microstructure. *Journal of Mammalian Evolution*  
1352 23: 221–235.
- 1353 Hulot M, Antoine PO. 2020. Mortality curves and population structures of late early  
1354 Miocene Rhinocerotidae (Mammalia, Perissodactyla) remains from the Béon 1 locality of  
1355 Montréal-du-Gers, France. *Palaeogeography, Palaeoclimatology, Palaeoecology*: 109938.
- 1356 Hutchinson JR. 2021. The evolutionary biomechanics of locomotor function in giant land  
1357 animals. *Journal of Experimental Biology* 224.
- 1358 Ives AR. 2019. R<sup>2</sup>s for Correlated Data: Phylogenetic Models, LMMs, and GLMMs. *Systematic*  
1359 *Biology* 68: 234–251.
- 1360 Janis CM, Shoshitaishvili B, Kambic R, Figueirido B. 2012. On their knees: distal femur  
1361 asymmetry in ungulates and its relationship to body size and locomotion. *Journal of*  
1362 *Vertebrate Paleontology* 32: 433–445.
- 1363 Jenkins FA, Camazine SM. 1977. Hip structure and locomotion in ambulatory and cursorial  
1364 carnivores. *Journal of Zoology* 181: 351–370.
- 1365 Kappelman J. 1988. Morphology and locomotor adaptations of the bovid femur in relation to  
1366 habitat. *Journal of Morphology* 198: 119–130.
- 1367 Klingenberg CP. 2008. Morphological Integration and Developmental Modularity. *Annual*  
1368 *Review of Ecology, Evolution, and Systematics* 39: 115–132.
- 1369 Klingenberg CP. 2014. Studying morphological integration and modularity at multiple levels:  
1370 concepts and analysis. *Philosophical Transactions of the Royal Society B: Biological Sciences*  
1371 369: 20130249.

- 1372 Klingenberg CP. 2016. Size, shape, and form: concepts of allometry in geometric  
1373 morphometrics. *Development Genes and Evolution* 226: 113–137.
- 1374 Klingenberg CP, Marugán-Lobón J. 2013. Evolutionary Covariation in Geometric  
1375 Morphometric Data: Analyzing Integration, Modularity, and Allometry in a Phylogenetic  
1376 Context. *Systematic Biology* 62: 591–610.
- 1377 Larramendi A. 2016. Shoulder height, body mass and shape of proboscideans. *Acta*  
1378 *Palaeontologica Polonica* 61: 537–574.
- 1379 Lessertisseur J, Saban R. 1967. Le squelette. Squelette appendiculaire. In: Grasset PP, ed.  
1380 *Traité de Zoologie. Tome XVI, Fascicule 1: Mammifères*. Paris, 298–1123.
- 1381 Liu S, Westbury MV, Dussex N, Mitchell KJ, Sinding MHS, Heintzman PD, Duchêne DA, Kapp  
1382 JD, Seth J von, Heiniger H, Sánchez-Barreiro F, Margaryan A, André-Olsen R, Cahsan BD,  
1383 Meng G, Yang C, Chen L, Valk T van der, Moodley Y, Rookmaaker K, Bruford MW, Ryder O,  
1384 Steiner C, Sonsbeek LGRB van, Vartanyan S, Guo C, Cooper A, Kosintsev P, Kirillova I, Lister  
1385 AM, Marques-Bonet T, Gopalakrishnan S, Dunn RR, Lorenzen ED, Shapiro B, Zhang G,  
1386 Antoine PO, Dalén L, Gilbert MTP. 2021. Ancient and modern genomes unravel the  
1387 evolutionary history of the rhinoceros family. *Cell* 184: 4874-4885.e16.
- 1388 Lu X. 2013. A juvenile skull of *Acerorhinus yuanmouensis* (Mammalia: Rhinocerotidae) from  
1389 the Late Miocene hominoid fauna of the Yuanmou Basin (Yunnan, China). *Geobios* 46: 539–  
1390 548.
- 1391 MacFadden BJ. 1998. Tale of two Rhinos: Isotopic Ecology, Paleodiet, and Niche  
1392 Differentiation of *Aphelops* and *Teloceras* from the Florida Neogene. *Paleobiology* 24: 274–  
1393 286.
- 1394 MacFadden BJ. 2005. Diet and habitat of toxodont megaherbivores (Mammalia,  
1395 Notoungulata) from the late Quaternary of South and Central America. *Quaternary Research*  
1396 64: 113–124.
- 1397 Mallet C, Billet G, Houssaye A, Cornette R. 2020. A first glimpse at the influence of body mass  
1398 in the morphological integration of the limb long bones: an investigation in modern  
1399 rhinoceroses. *Journal of Anatomy* 237: 704–726.
- 1400 Mallet C, Cornette R, Billet G, Houssaye A. 2019. Interspecific variation in the limb long  
1401 bones among modern rhinoceroses—extent and drivers. *PeerJ* 7: e7647.
- 1402 Mallet C, Houssaye A, Cornette R, Billet G. In Press. Long bone shape variation in the  
1403 forelimb of Rhinocerotoida – Relation with size, body mass and body proportions.  
1404 *Zoological Journal of the Linnean Society*: 1–33.
- 1405 Mallison H, Wings O. 2014. Photogrammetry in Paleontology - A practical guide. *Journal of*  
1406 *Paleontological Techniques*: 1–31.



- 1407 Martins EP, Hansen TF. 1997. Phylogenies and the Comparative Method: A General  
1408 Approach to Incorporating Phylogenetic Information into the Analysis of Interspecific Data.  
1409 *The American Naturalist* 149: 646–667.
- 1410 Martín-Serra A, Benson RBJ. 2019. Developmental constraints do not influence long-term  
1411 phenotypic evolution of marsupial forelimbs as revealed by interspecific disparity and  
1412 integration patterns. *The American Naturalist*.
- 1413 McGhee RB, Frank AA. 1968. On the stability properties of quadruped creeping gaits.  
1414 *Mathematical Biosciences* 3: 331–351.
- 1415 Mead AJ. 2000. Sexual dimorphism and paleoecology in *Teleoceras*, a North American  
1416 Miocene rhinoceros. *Paleobiology* 26: 689–706.
- 1417 Mihlbachler MC. 2003. Demography of Late Miocene Rhinoceroses (*Teleoceras proterum*  
1418 and *Aphelops malacorhinus*) from Florida: Linking Mortality and Sociality in Fossil  
1419 Assemblages. *Paleobiology* 29: 412–428.
- 1420 Mihlbachler MC. 2007. Sexual Dimorphism and Mortality Bias in a Small Miocene North  
1421 American Rhino, *Menoceras arikareense*: Insights into the Coevolution of Sexual Dimorphism  
1422 and Sociality in Rhinos. *Journal of Mammalian Evolution* 14: 217–238.
- 1423 Mitteroecker P, Gunz P, Windhager S, Schaefer K. 2013. A brief review of shape, form, and  
1424 allometry in geometric morphometrics, with applications to human facial morphology.  
1425 *Hystrix, the Italian Journal of Mammalogy* 24: 59–66.
- 1426 Orlando L, Leonard JA, Thenot A, Laudet V, Guerin C, Hänni C. 2003. Ancient DNA analysis  
1427 reveals woolly rhino evolutionary relationships. *Molecular Phylogenetics and Evolution* 28:  
1428 485–499.
- 1429 Osborn HF. 1900. The Angulation of the Limbs of Proboscidea, Dinocerata, and Other  
1430 Quadrupeds, in Adaptation to Weight. *The American Naturalist* 34: 89–94.
- 1431 Osborn HF. 1929. *The Titanotheres of ancient Wyoming, Dakota, and Nebraska*. Government  
1432 Printing Office.
- 1433 Panagiotopoulou O, Pataky TC, Hutchinson JR. 2019. Foot pressure distribution in White  
1434 Rhinoceroses (*Ceratotherium simum*) during walking. *PeerJ* 7: e6881.
- 1435 Paradis E, Blomberg SP, Bolker B, Brown J, Claude J, Cuong HS, Desper R, Didier G, Durand B,  
1436 Dutheil J, Ewing J, Gascuel O, Guillaume T, Heibl C, Ives A, Jones B, Krah F, Lawson D, Lefort V,  
1437 Legendre P, Lemon J, Marcon E, McCloskey R, Nylander J, Opgen-Rhein R, Popescu AA,  
1438 Royer-Carenzi M, Schliep K, Strimmer K, de Vienne D. 2018. *Ape: Analyses of Phylogenetics*  
1439 *and Evolution*.
- 1440 Paul GS. 1997. Dinosaur models: the Good, the Bad, and using them to estimate the mass of  
1441 dinosaurs. *Dinofest International: Proceedings of a Symposium held at Arizona State*  
1442 *University*. The Academy of Natural Sciences, Philadelphia, PA, USA: D.L.Wolberg, E.Stump &  
1443 G.Rosenberg, 129–154.

- 1444 Paul GS, Christiansen P. 2000. Forelimb posture in neoceratopsian dinosaurs: implications for  
1445 gait and locomotion. *Paleobiology* 26: 450–465.
- 1446 Piras P, Maiorino L, Raia P, Marcolini F, Salvi D, Vignoli L, Kotsakis T. 2010. Functional and  
1447 phylogenetic constraints in Rhinocerotinae craniodental morphology. *Evolutionary Ecology*  
1448 *Research* 12: 897–928.
- 1449 Polly PD. 2007. Limbs in mammalian evolution. Chapter 15. In: Hall BK, ed. *Fins into Limbs:*  
1450 *Evolution, Development, and Transformation*. Chicago: Brian K. Hall, 245–268.
- 1451 Price SA, Bininda-Emonds ORP. 2009. A comprehensive phylogeny of extant horses, rhinos  
1452 and tapirs (Perissodactyla) through data combination. *Zoosystematics and Evolution* 85:  
1453 277–292.
- 1454 Prothero DR. 1998. Hyracodontidae. In: Janis CM, Scott KM, Jacobs LL, eds. *Evolution of*  
1455 *Tertiary Mammals of North America: Volume 1, Terrestrial Carnivores, Ungulates, and*  
1456 *Ungulate Like Mammals*. Cambridge University Press, 589–593.
- 1457 Prothero DR. 2005. *The Evolution of North American Rhinoceroses*. Cambridge.
- 1458 Prothero DR. 2013. *Rhinoceros Giants: The Paleobiology of Indricotheres*. Bloomington and  
1459 Indianapolis.
- 1460 Prothero DR, Schoch RM. 1989. *The evolution of perissodactyls*. New York: Oxford University  
1461 Press.
- 1462 Prothero DR, Sereno PC. 1982. Allometry and Paleoecology of Medial Miocene Dwarf  
1463 Rhinoceroses from the Texas Gulf Coastal Plain. *Paleobiology* 8: 16–30.
- 1464 Qiu ZX, Wang BY. 2007. Paraceratheres Fossils of China. *Palaeontologia Sinica, newseries C*  
1465 29: 1–396.
- 1466 R Core Team. 2014. *R: a language and environment for statistical computing*. Vienna: R  
1467 Foundation for Statistical Computing.
- 1468 Raia P, Carotenuto F, Passaro F, Fulgione D, Fortelius M. 2012. Ecological Specialization in  
1469 Fossil Mammals Explains Cope’s Rule. *The American Naturalist* 179: 328–337.
- 1470 Regnault S, Hermes R, Hildebrandt T, Hutchinson J, Weller R. 2013. Osteopathology in the  
1471 feet of rhinoceroses: lesion type and distribution. *Journal of Zoo and Wildlife Medicine* 44:  
1472 918–927.
- 1473 Ren L, Miller CE, Lair R, Hutchinson JR. 2010. Integration of biomechanical compliance,  
1474 leverage, and power in elephant limbs. *Proceedings of the National Academy of Sciences*  
1475 107: 7078–7082.
- 1476 Revell LJ. 2012. phytools: an R package for phylogenetic comparative biology (and other  
1477 things). *Methods in Ecology and Evolution* 3: 217–223.

- 1478 Robinet C, Remy JA, Laurent Y, Danilo L, Lihoreau F. 2015. A new genus of Lophiodontidae  
1479 (Perissodactyla, Mammalia) from the early Eocene of La Borie (Southern France) and the  
1480 origin of the genus Lophiodon Cuvier, 1822. *Geobios* 48: 25–38.
- 1481 Rohlf FJ. 2001. Comparative Methods for the Analysis of Continuous Variables: Geometric  
1482 Interpretations. *Evolution* 55: 2143–2160.
- 1483 Rohlf FJ, Slice D. 1990. Extensions of the Procrustes Method for the Optimal Superimposition  
1484 of Landmarks. *Systematic Biology* 39: 40–59.
- 1485 Scherler L, Mennecart B, Hiard F, Becker D. 2013. Evolutionary history of hoofed mammals  
1486 during the Oligocene–Miocene transition in Western Europe. *Swiss Journal of Geosciences*  
1487 106: 349–369.
- 1488 Schlager S. 2017. Chapter 9 - Morpho and Rvcg – Shape Analysis in R: R-Packages for  
1489 Geometric Morphometrics, Shape Analysis and Surface Manipulations. In: Zheng G, Li S,  
1490 Székely G, eds. *Statistical Shape and Deformation Analysis*. Academic Press, 217–256.
- 1491 Schliep KP. 2011. phangorn: phylogenetic analysis in R. *Bioinformatics* 27: 592–593.
- 1492 Schmidt M, Fischer MS. 2009. Morphological Integration in Mammalian Limb Proportions:  
1493 Dissociation Between Function and Development. *Evolution* 63: 749–766.
- 1494 Serio C, Raia P, Meloro C. 2020. Locomotory Adaptations in 3D Humerus Geometry of  
1495 Xenarthra: Testing for Convergence. *Frontiers in Ecology and Evolution* 8.
- 1496 Steiner CC, Ryder OA. 2011. Molecular phylogeny and evolution of the Perissodactyla.  
1497 *Zoological Journal of the Linnean Society* 163: 1289–1303.
- 1498 Stilson KT, Hopkins SSB, Davis EB. 2016. Osteopathology in Rhinocerotidae from 50 Million  
1499 Years to the Present. *PLOS ONE* 11: e0146221.
- 1500 Swenson N. 2014. *Functional and Phylogenetic Ecology in R*. New York: Springer-Verlag.
- 1501 Thermo Fisher Scientific. 2018. *Avizo*.
- 1502 Tissier J, Antoine PO, Becker D. 2020. New material of *Epiaceratherium* and a new species of  
1503 *Mesaceratherium* clear up the phylogeny of early Rhinocerotidae (Perissodactyla). *Royal*  
1504 *Society Open Science* 7: 200633.
- 1505 Tissier J, Becker D, Codrea V, Costeur L, Fărcaș C, Solomon A, Venczel M, Maridet O. 2018.  
1506 New data on Aymnodontidae (Mammalia, Perissodactyla) from Eastern Europe: Phylogenetic  
1507 and palaeobiogeographic implications around the Eocene-Oligocene transition. *PLOS ONE*  
1508 13: e0193774.
- 1509 Tougaard C, Delefosse T, Hänni C, Montgelard C. 2001. Phylogenetic Relationships of the Five  
1510 Extant Rhinoceros Species (Rhinocerotidae, Perissodactyla) Based on Mitochondrial  
1511 Cytochrome b and 12S rRNA Genes. *Molecular Phylogenetics and Evolution* 19: 34–44.

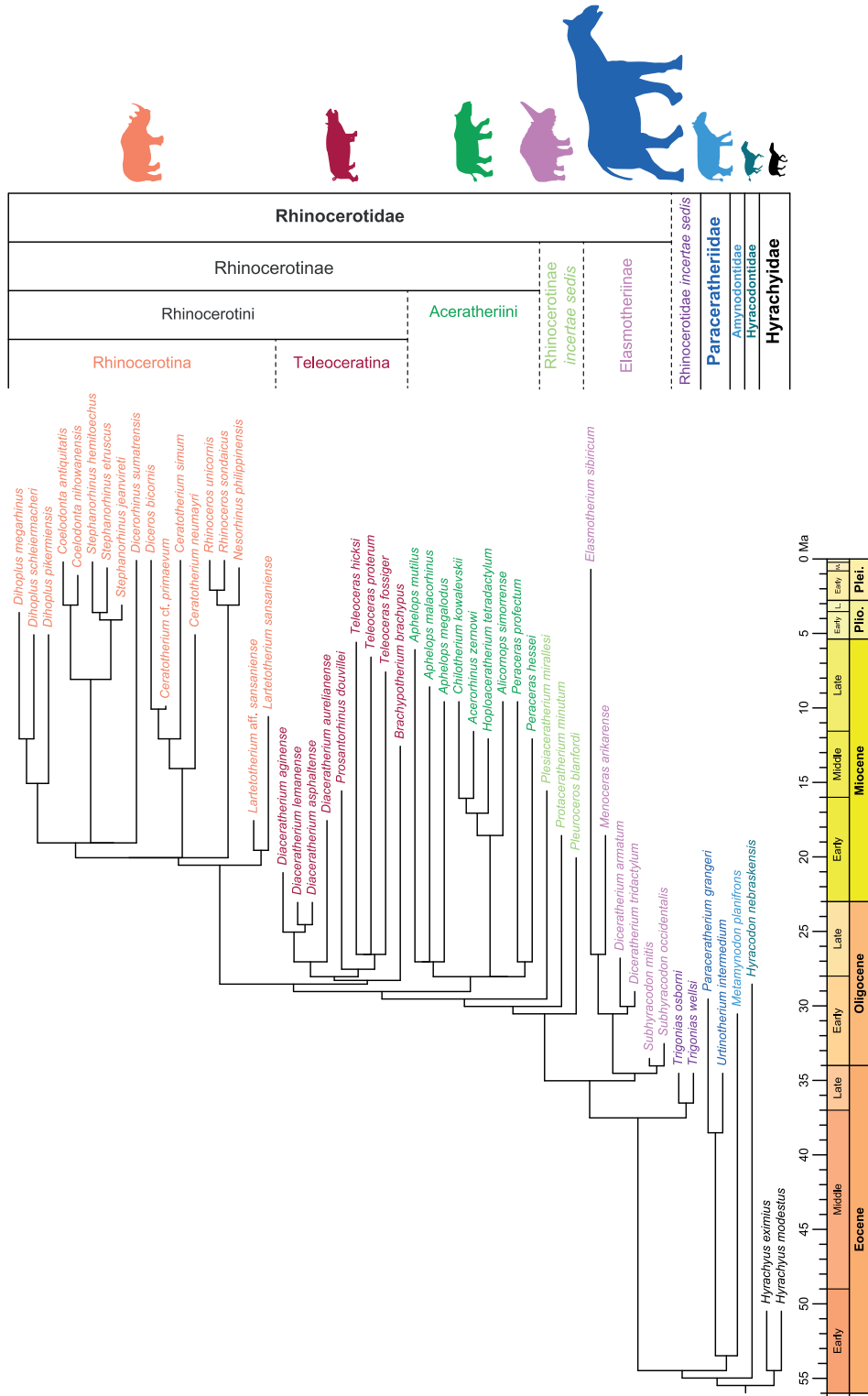
- 1512 Tsai HP, Holliday CM. 2015. Articular soft tissue anatomy of the archosaur hip joint:  
1513 Structural homology and functional implications. *Journal of Morphology* 276: 601–630.
- 1514 Wang H, Bai B, Meng J, Wang Y. 2016. Earliest known unequivocal rhinocerotoid sheds new  
1515 light on the origin of Giant Rhinos and phylogeny of early rhinocerotoids. *Scientific Reports* 6.
- 1516 Wang B, Secord R. 2020. Paleoecology of *Aphelops* and *Teleoceras* (Rhinocerotidae) through  
1517 an interval of changing climate and vegetation in the Neogene of the Great Plains, central  
1518 United States. *Palaeogeography, Palaeoclimatology, Palaeoecology* 542: 109411.
- 1519 Wasserstein RL, Schirm AL, Lazar NA. 2019. Moving to a World Beyond “ $p < 0.05$ ”. *The*  
1520 *American Statistician* 73: 1–19.
- 1521 Welker F, Collins MJ, Thomas JA, Wadsley M, Brace S, Cappellini E, Turvey ST, Reguero M,  
1522 Gelfo JN, Kramarz A, Burger J, Thomas-Oates J, Ashford DA, Ashton PD, Rowsell K, Porter  
1523 DM, Kessler B, Fischer R, Baessmann C, Kaspar S, Olsen JV, Kiley P, Elliott JA, Kelstrup CD,  
1524 Mullin V, Hofreiter M, Willerslev E, Hublin JJ, Orlando L, Barnes I, MacPhee RDE. 2015.  
1525 Ancient proteins resolve the evolutionary history of Darwin’s South American ungulates.  
1526 *Nature* 522: 81–84.
- 1527 Welker F, Smith GM, Hutson JM, Kindler L, Garcia-Moreno A, Villaluenga A, Turner E,  
1528 Gaudzinski-Windheuser S. 2017. Middle Pleistocene protein sequences from the rhinoceros  
1529 genus *Stephanorhinus* and the phylogeny of extant and extinct Middle/Late Pleistocene  
1530 Rhinocerotidae. *PeerJ* 5: e3033.
- 1531 Wiley DF, Amenta N, Alcantara DA, Ghosh D, Kil YJ, Delson E, Harcourt-Smith W, Rohlf FJ, St.  
1532 John K, Hamann B. 2005. Evolutionary Morphing. *Proceedings of IEEE Visualization 2005*.  
1533 Minneapolis, Minnesota.
- 1534 Willerslev E, Gilbert MTP, Binladen J, Ho SY, Campos PF, Ratan A, Tomsho LP, da Fonseca RR,  
1535 Sher A, Kuznetsova TV, Nowak-Kemp M, Roth TL, Miller W, Schuster SC. 2009. Analysis of  
1536 complete mitochondrial genomes from extinct and extant rhinoceroses reveals lack of  
1537 phylogenetic resolution. *BMC Evolutionary Biology* 9: 1–11.
- 1538 Yilmaz S. 1998. Macro-anatomical investigations on the skeletons of porcupine (*Hystrix*  
1539 *cristata*). Part III: skeleton axiale. *Anatomia, histologia, embryologia* 27: 293–296.
- 1540 Young NM, Hallgrímsson B. 2005. Serial Homology and the Evolution of Mammalian Limb  
1541 Covariation Structure. *Evolution* 59: 2691–2704.
- 1542 Yuan J, Sheng G, Hou X, Shuang X, Yi J, Yang H, Lai X. 2014. Ancient DNA sequences from  
1543 *Coelodonta antiquitatis* in China reveal its divergence and phylogeny. *Science China Earth*  
1544 *Sciences* 57: 388–396.
- 1545 Zelditch ML, Swiderski DL, Sheets HD, Fink WL. 2012. *Geometric morphometrics for*  
1546 *biologists: A Primer*. Academic Press.

1547 Zschokke S, Baur B. 2002. Inbreeding, outbreeding, infant growth, and size dimorphism in  
1548 captive Indian rhinoceros (*Rhinoceros unicornis*). *Canadian Journal of Zoology* 80: 2014–  
1549 2023.

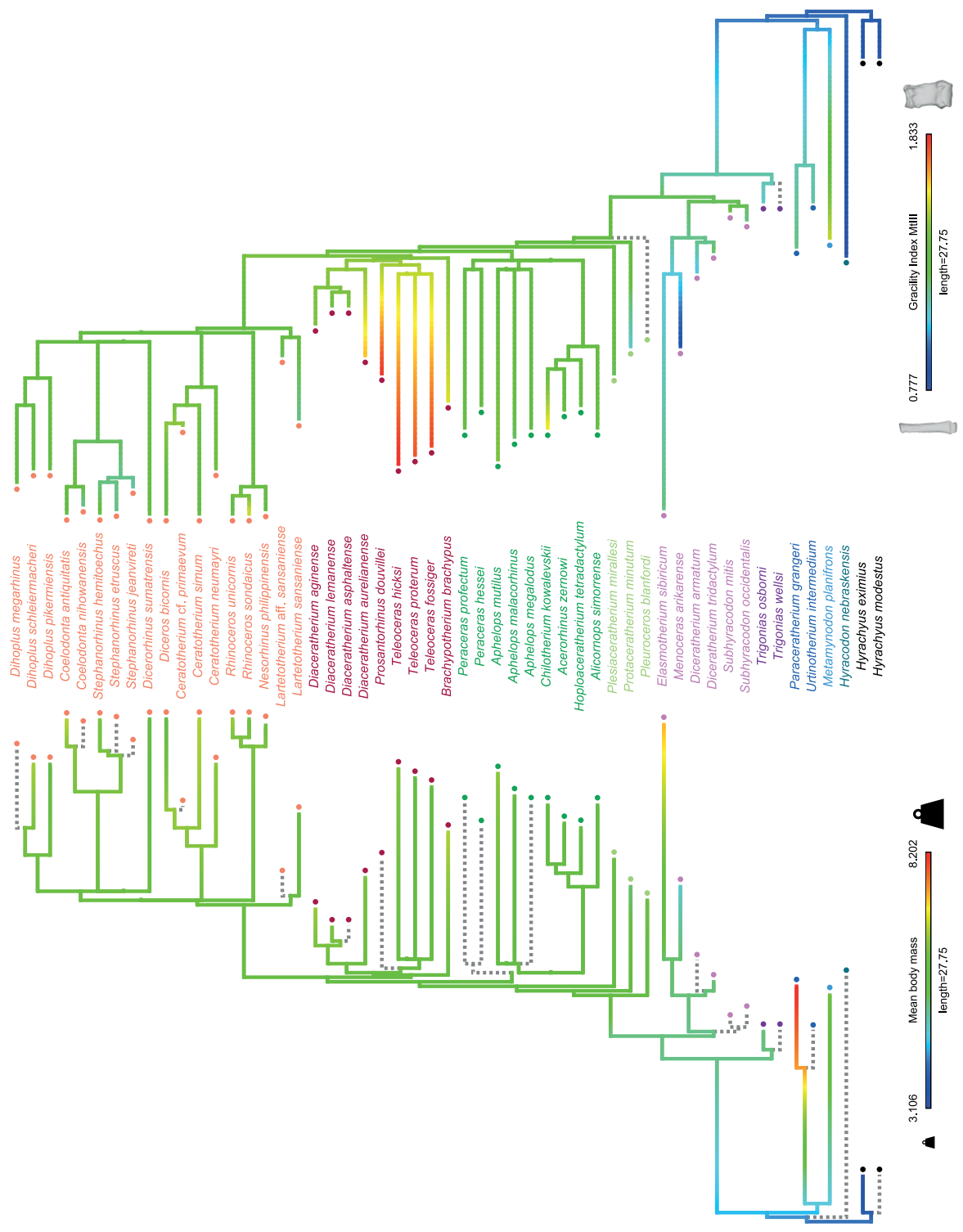
1550

1551 **FIGURES**

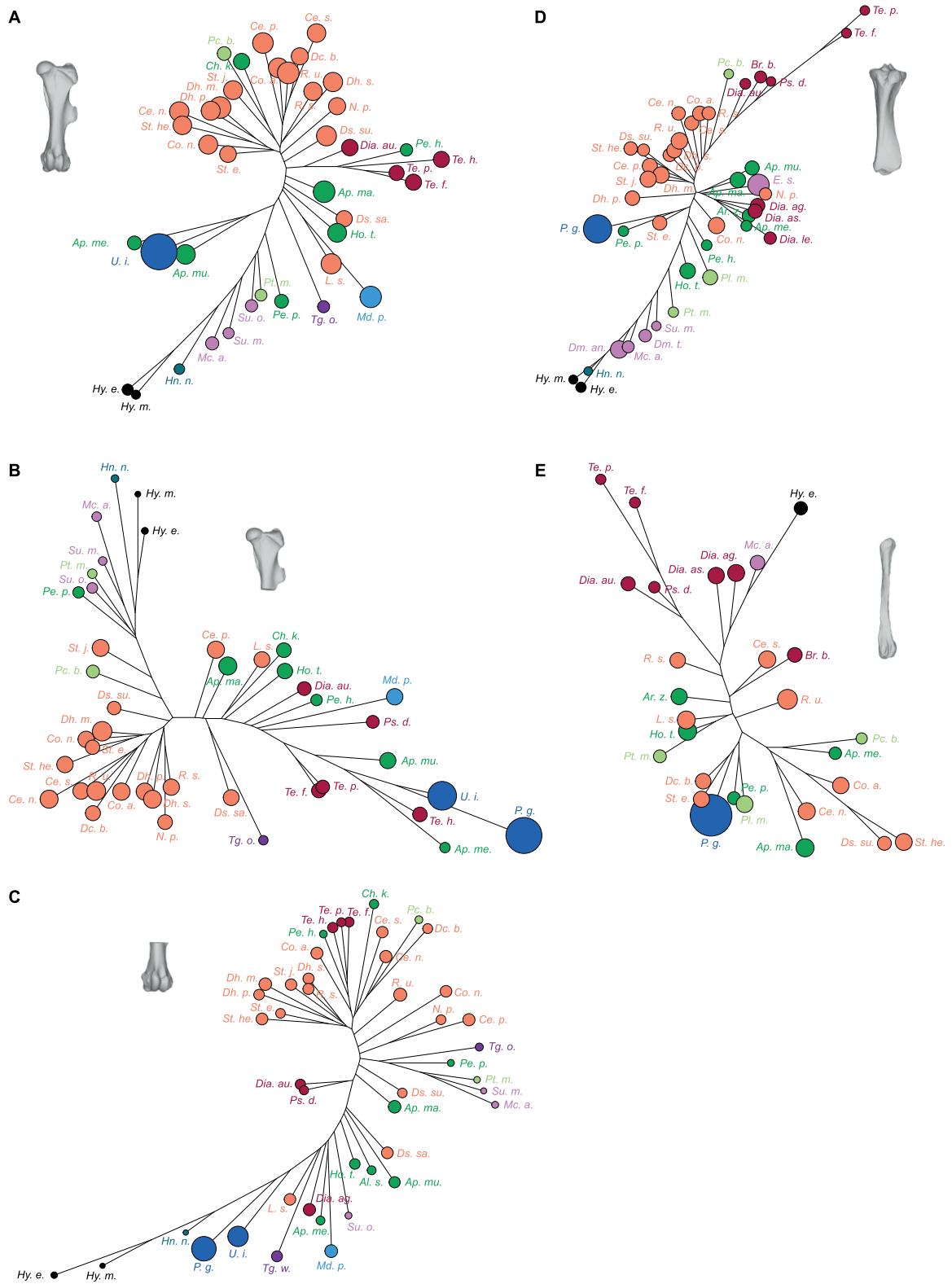
1552 **Figure 1.** Composite cladogram of the studied species. Families, subfamilies, tribes and subtribes are  
 1553 defined by a colour code following the cladistic framework of Antoine *et al.* (2003) and Becker *et al.*  
 1554 (2013). All silhouettes representing a member of each group are at scale (provided by  
 1555 [www.phylopic.org](http://www.phylopic.org) under Creative Commons license).



1557 **Figure 2.** Evolution of BM and GI-MT3 along the phylogeny for the studied species. Left: mean BM;  
 1558 Right: mean GI-MT3. Computations were made on log-transformed cubic root of mean BM (BM) and  
 1559 log-transformed GI-MT3. Values at nodes and along branches were reconstructed based on a  
 1560 Brownian motion model of evolution (Revell, 2012). Colour code for taxa follows Figure 1. Evolution  
 1561 of the third metatarsal shape depending on the GI-MT3 value is illustrated by specimens *Hyrachyus*  
 1562 *eximius* AMNH FM 12675 (minimum) and *Teleoceras fossiger* YPM VP 039358 (maximum).

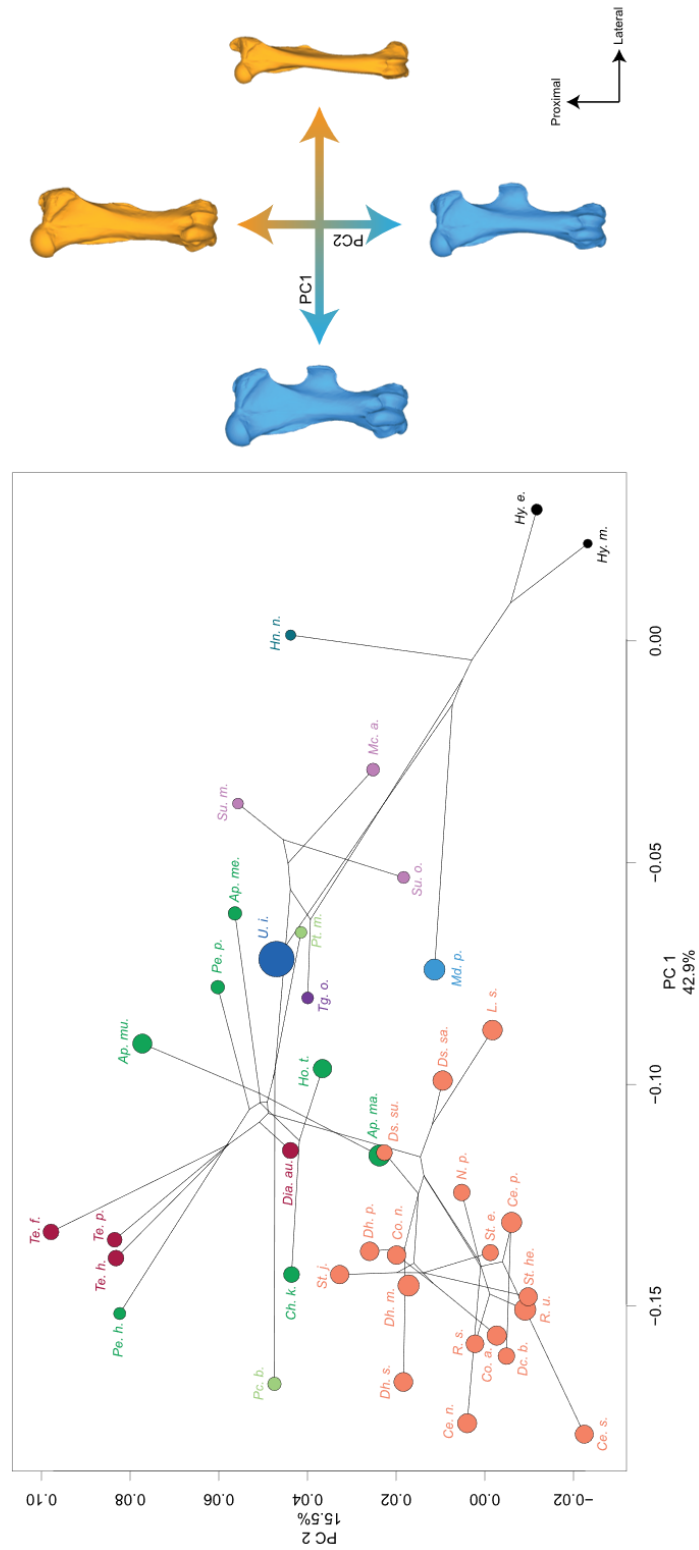


1564 **Figure 3.** Neighbour Joining trees computed on all PC scores obtained from the PCAs performed on  
 1565 shape data. Colour code follows Figure 1 and abbreviations follow Table 1. Point size is proportional  
 1566 to the mean log centroid size of each species. **A:** complete femur; **B:** proximal partial femur; **C:** distal  
 1567 partial femur; **D:** tibia; **E:** fibula.



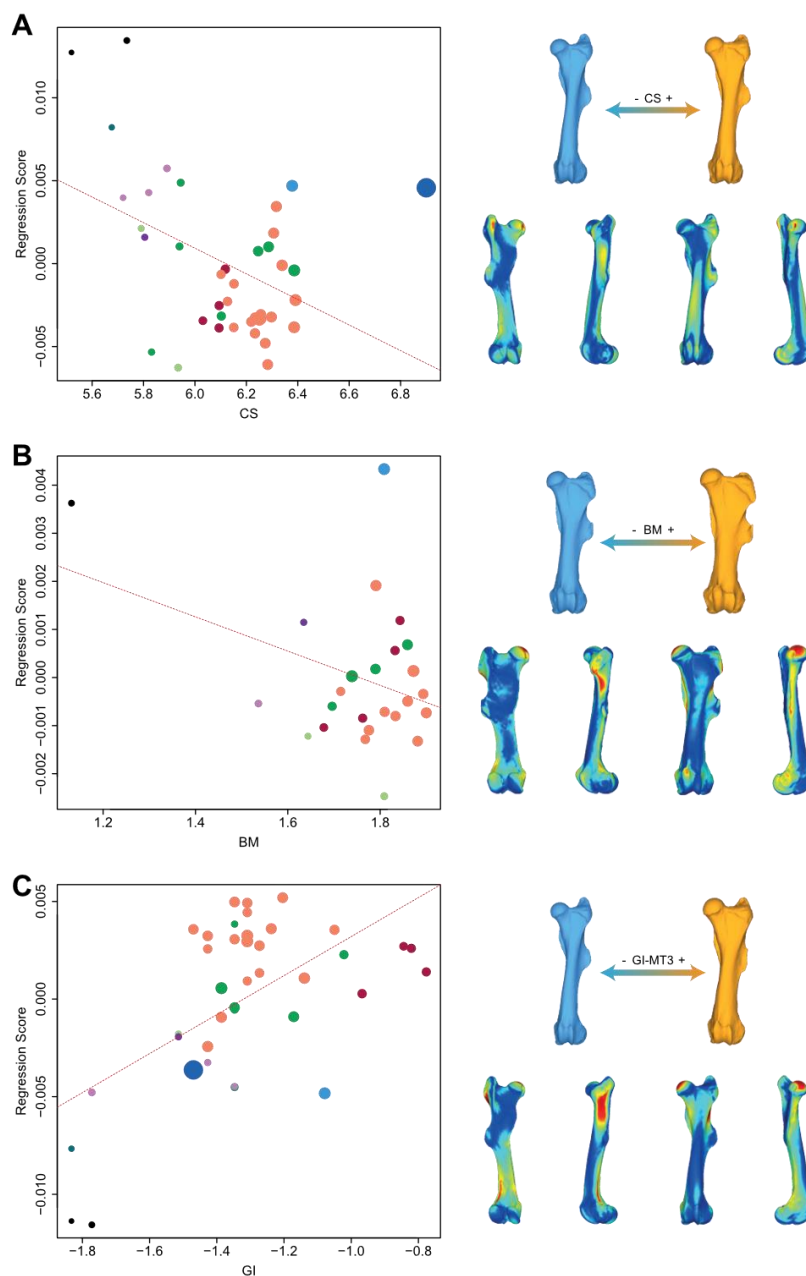


1569 **Figure 4.** Results of the PCA performed on morphometric data of the complete femur and shape  
 1570 variation associated with the first axis of the PCA (cranial view). Blue: negative side of the axis.  
 1571 Orange: positive side of the axis. Phylogenetic relationships are plotted in the morphospace. Colour  
 1572 code follows Figure 1 and abbreviations follow Table 1. Point size is proportional to the mean log  
 1573 centroid size of each species.



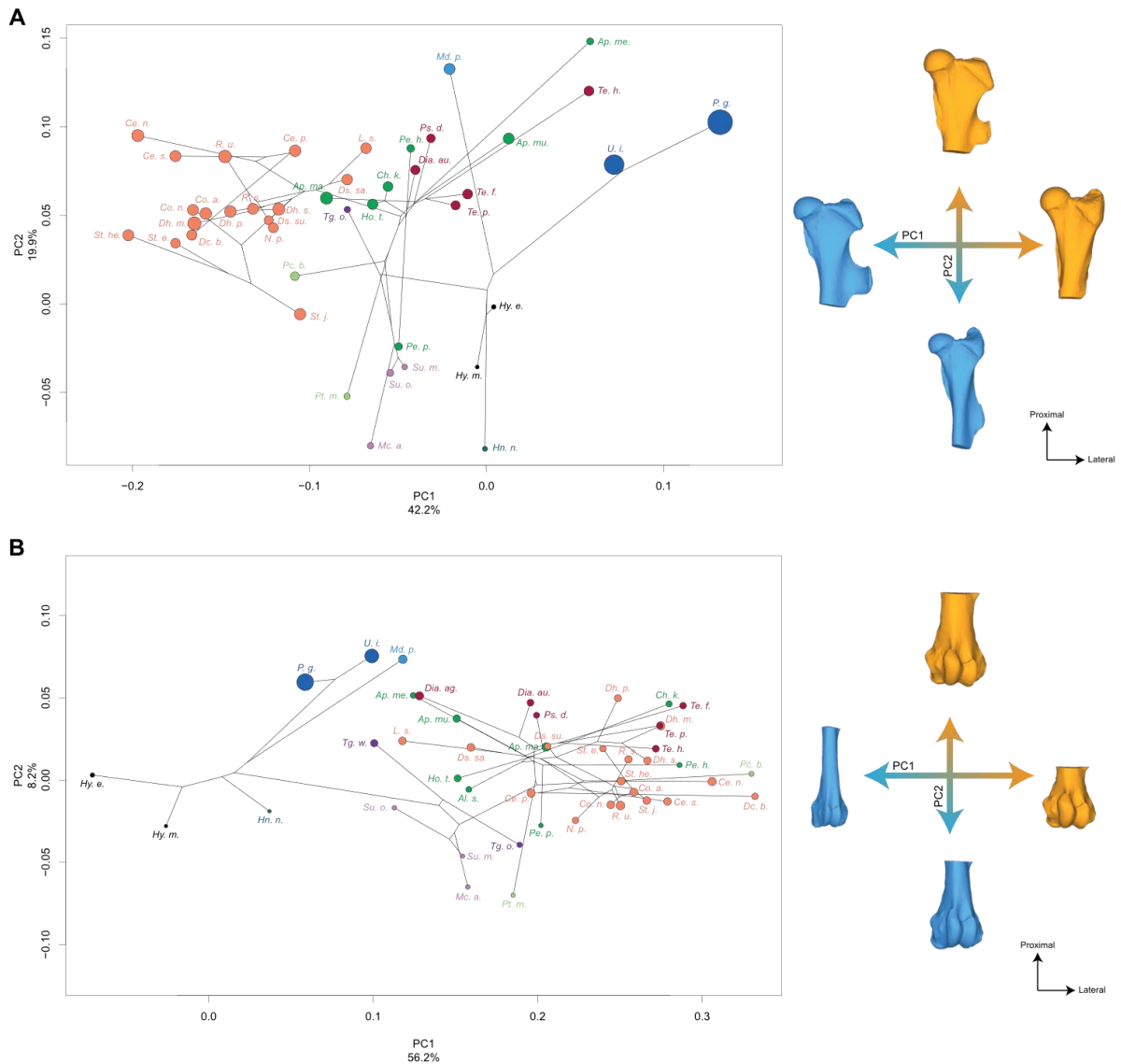
1574

1575 **Figure 5.** Significant PGLS regression plots for complete femur performed on shape data and log-  
 1576 transformed centroid size (CS) (A), log-transformed cubic root of mean body mass (BM) (B), log-  
 1577 transformed mean gracility index (GI-MT3) (C). Points colour code follows Figure 1. Point size is  
 1578 proportional to mean log CS of each species. On the right, shapes associated with minimum and  
 1579 maximum fitted values (top row) and colour maps of the location and intensity of the shape  
 1580 deformation (bottom row). Blue: minimum value of the regression. Orange: maximum value of the  
 1581 regression. For each bone, the shape associated with the minimum was coloured depending on its  
 1582 distance to the shape associated with the maximum (blue indicates a low deformation intensity and  
 1583 red indicates a high deformation intensity). Orientation from left to right in each case: caudal, lateral,  
 1584 cranial and medial.



1585

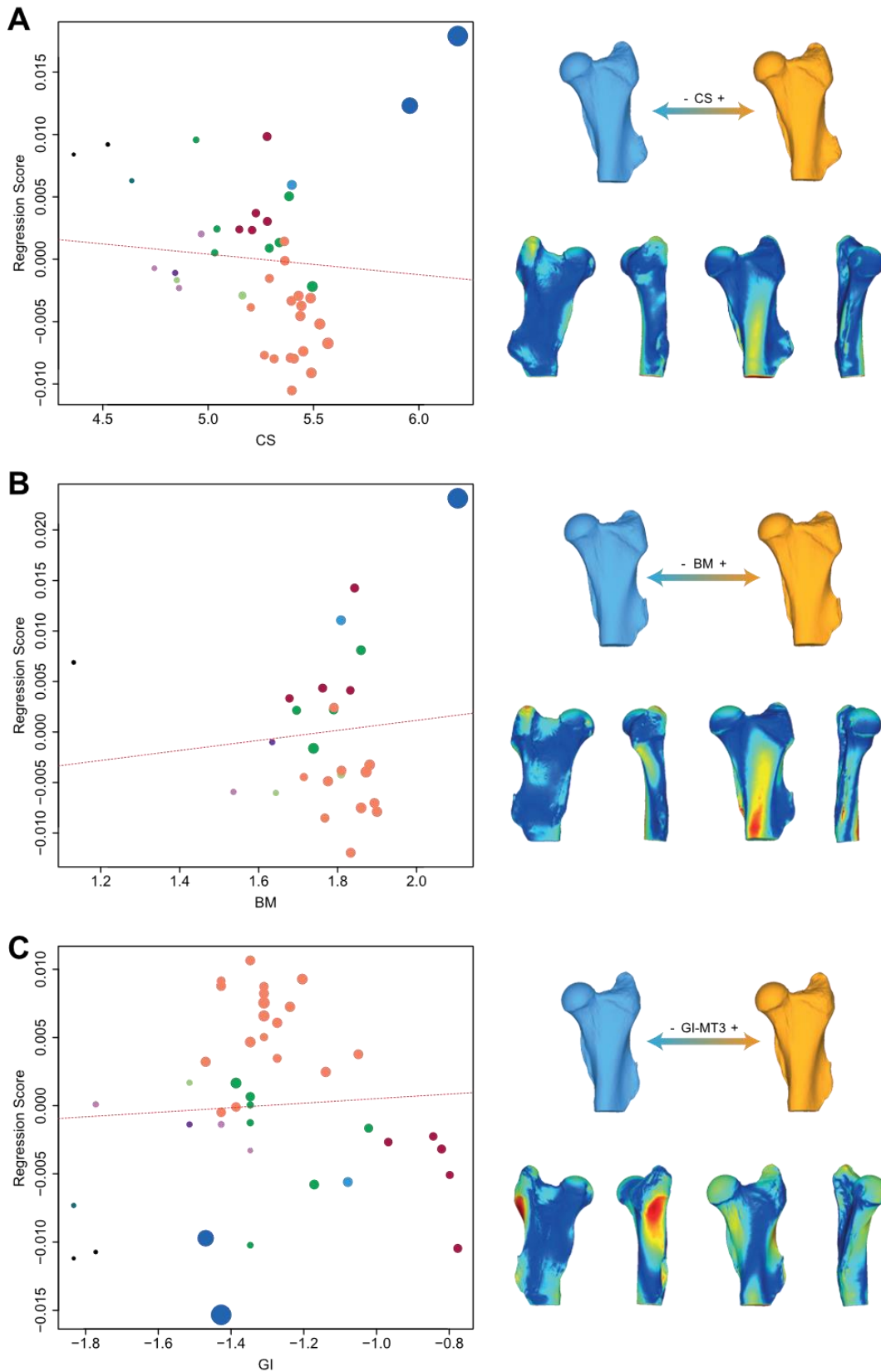
1586 **Figure 6.** Results of the PCA performed on morphometric data of proximal partial femur (A) and  
 1587 distal partial femur (B) and shape variation associated with the first two axes of the PCA (caudal  
 1588 view). Blue: negative side of the axis. Orange: positive side of the axis. Phylogenetic relationships are  
 1589 plotted in the morphospace. Colour code follows Figure 1 and abbreviations follow Table 1. Point size  
 1590 is proportional to the mean log centroid size of each species.



1591

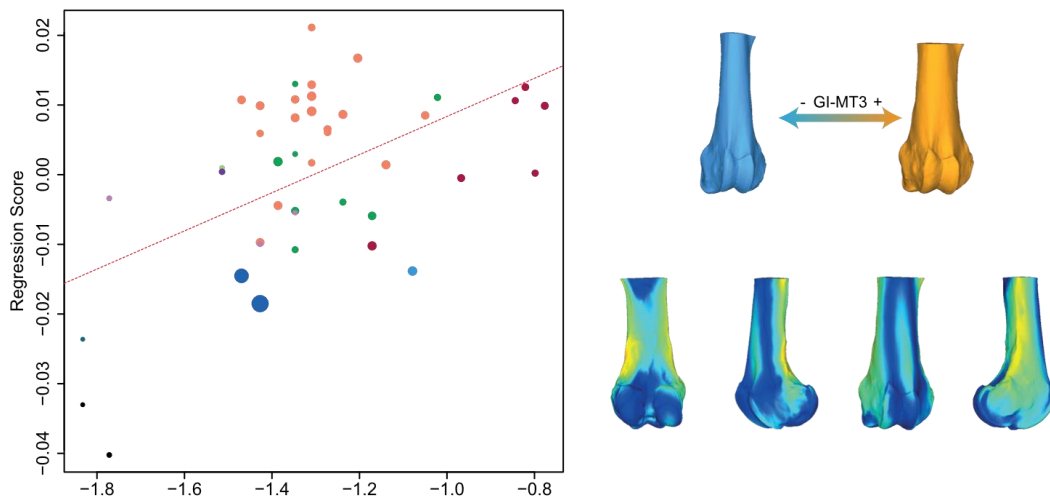
1592 **Figure 7.** Significant PGLS regression plots for proximal partial femur performed on shape data and  
 1593 log-transformed centroid size (CS) (A), log-transformed cubic root of mean body mass (BM) (B), log-  
 1594 transformed mean gracility index (GI-MT3) (C). Points colour code follows Figure 1. Point size is  
 1595 proportional to mean log CS of each species. On the right, shapes associated with minimum and  
 1596 maximum fitted values (top row) and colour maps of the location and intensity of the shape  
 1597 deformation (bottom row). Blue: minimum value of the regression. Orange: maximum value of the  
 1598 regression. For each bone, the shape associated with the minimum was coloured depending on its

1599 distance to the shape associated with the maximum (blue indicates a low deformation intensity and  
1600 red indicates a high deformation intensity). Orientation from left to right in each case: caudal, lateral,  
1601 cranial and medial.



1602

1603 **Figure 8.** Significant PGLS regression plots for distal partial femur performed on shape data and log-  
1604 transformed mean gracility index (GI-MT3). Points colour code follows Figure 1. Point size is  
1605 proportional to mean log CS of each species. On the right, shapes associated with minimum and  
1606 maximum fitted values (top row) and colour maps of the location and intensity of the shape  
1607 deformation (bottom row). Blue: minimum value of the regression. Orange: maximum value of the  
1608 regression. For each bone, the shape associated with the minimum was coloured depending on its  
1609 distance to the shape associated with the maximum (blue indicates a low deformation intensity and  
1610 red indicates a high deformation intensity). Orientation from left to right in each case: caudal, lateral,  
1611 cranial and medial.

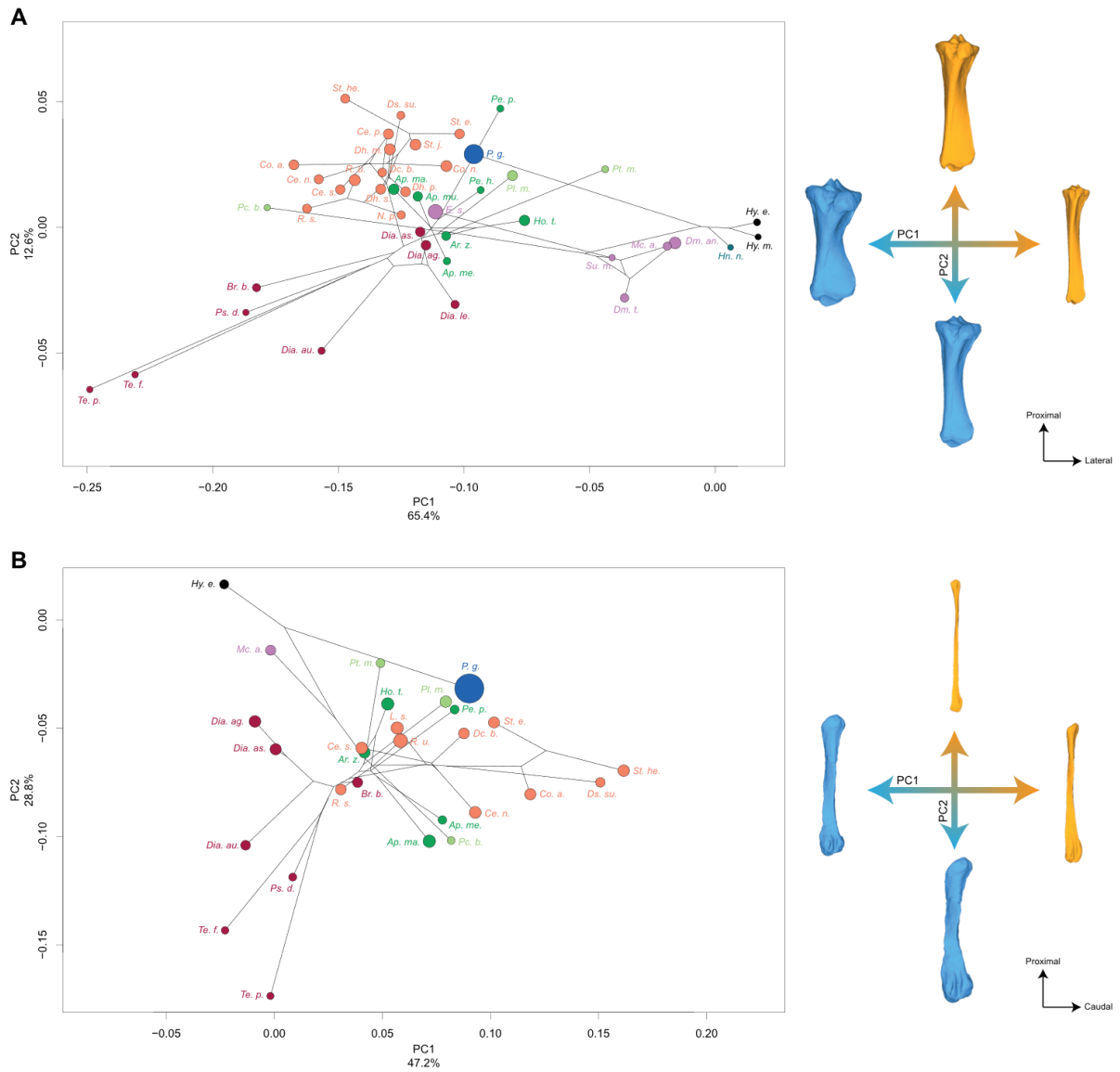


1612

1613

1614

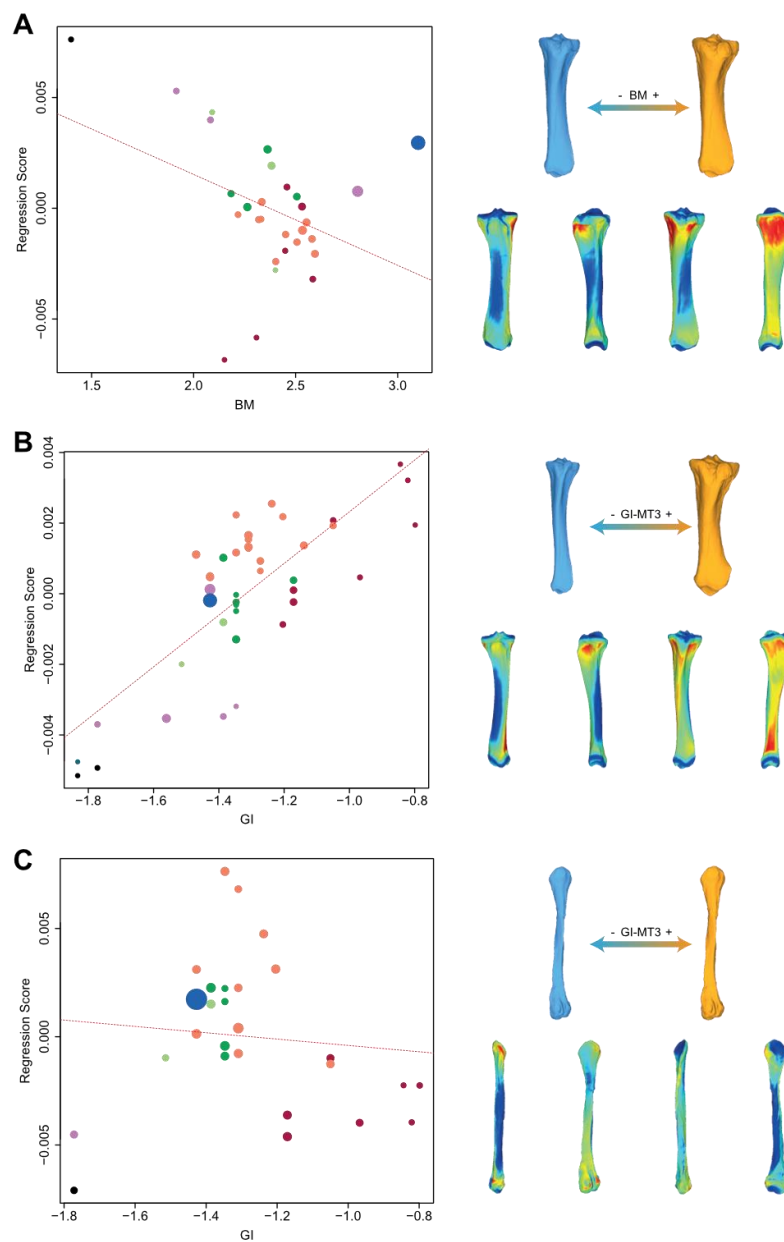
1615 **Figure 9.** Results of the PCA performed on morphometric data of tibia (A) and fibula (B) and shape  
 1616 variation associated with the first two axes of the PCA (caudal view). Blue: negative side of the axis.  
 1617 Orange: positive side of the axis. Phylogenetic relationships are plotted in the morphospace. Colour  
 1618 code follows Figure 1 and abbreviations follow Table 1. Point size is proportional to the mean log  
 1619 centroid size of each species.



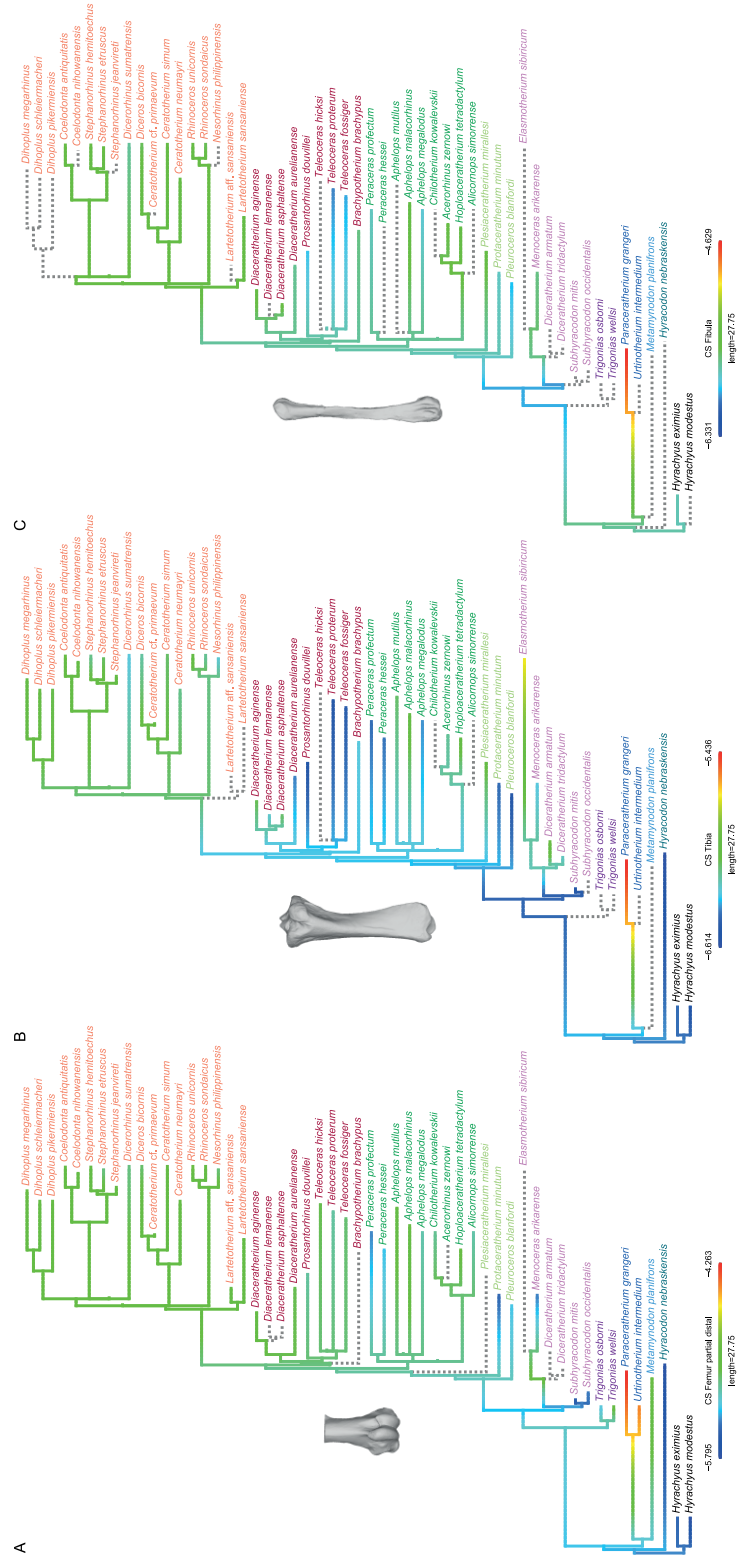
1620

1621

1622 **Figure 10.** Significant PGLS regression plots for tibia performed on shape data and log-transformed  
 1623 cubic root of mean body mass (BM) (A) and log-transformed mean gracility index (GI-MT3) (B), and  
 1624 fibula performed on shape data and log-transformed mean gracility index (GI-MT3) (C). Points colour  
 1625 code follows Figure 1. Point size is proportional to mean log CS of each species. On the right, shapes  
 1626 associated with minimum and maximum fitted values (top row) and colour maps of the location and  
 1627 intensity of the shape deformation (bottom row). Blue: minimum value of the regression. Orange:  
 1628 maximum value of the regression. For each bone, the shape associated with the minimum was  
 1629 coloured depending on its distance to the shape associated with the maximum (blue indicates a low  
 1630 deformation intensity and red indicates a high deformation intensity). Orientation from left to right  
 1631 in each case: caudal, lateral, cranial and medial.

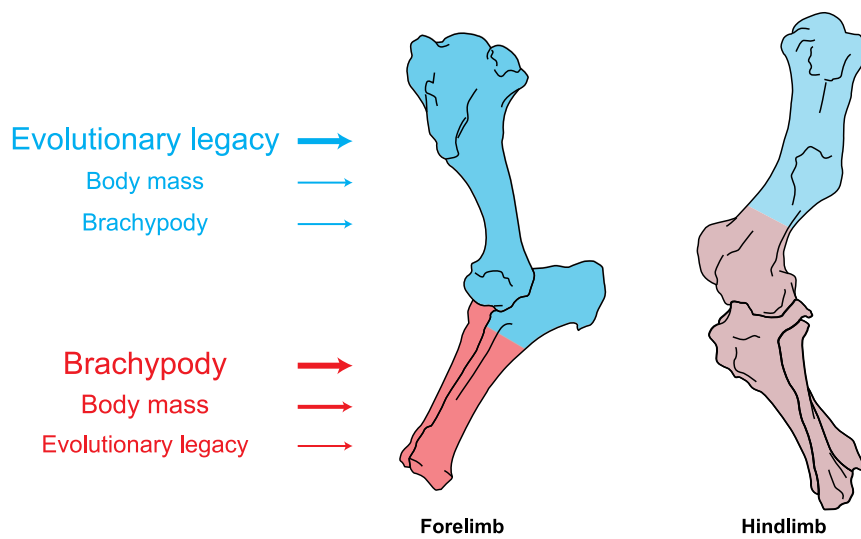


1633 **Figure 11.** Evolution of centroid size (CS) along the phylogeny for the studied species. **A:** distal partial  
 1634 femur, **B:** tibia, **C:** fibula. The cladogram used here is the same composite one as used in Figure 1.  
 1635 Computations were made on log-transformed CS. Values at nodes and along branches were  
 1636 reconstructed based on a Brownian motion model of evolution (Revell, 2012). Colour code for taxa  
 1637 follows Figure 1.





1639 **Figure 12.** Schematic summary of the relations between bone shape and the different variables  
1640 tested in this work and in Mallet *et al.* (in press). Blue indicates a shape variation dominated by  
1641 evolutionary legacy over other parameters. Red indicates a shape variation mainly dominated by  
1642 brachypody and/or body mass over other parameters. This relative influence is based on the results  
1643 obtained through the NJ trees, the PCA and the regression plots of the PGLS described in the  
1644 previous chapters. The size of the font and arrows for each variable is proportional to its relation  
1645 with the shape for each bone or part of bone based on the overall previous results. Faded colours on  
1646 the hind limb indicate a lower association with body mass in general. Bones modified from  
1647 Archeozoo.org under Creative Commons license.



1648

1650 **Table 1.** List of the abbreviations, mean body masses and gracility indexes used in this study. Sources  
 1651 used to compile mean body mass and gracility index are given in Supplementary Table S2.

Taxon	Abbreviation	Mean body mass (kg)	Gracility Index (MtIII)
<i>Acerorhinus zernowi</i>	Ar. z.	700	0.26
<i>Alicornops simorreense</i>	Al. s.	875	0.29
<i>Aphelops malacorhinus</i>	Ap. ma.	889	0.25
<i>Aphelops megalodus</i>	Ap. me.	NA	0.26
<i>Aphelops mutilus</i>	Ap. mu.	1840	0.31
<i>Brachypotherium brachypus</i>	Br. b.	2327	0.35
<i>Ceratotherium cf. primaevum</i>	Ce. p.	NA	0.32
<i>Ceratotherium neumayri</i>	Ce. n.	1843	0.30
<i>Ceratotherium simum</i>	Ce. s.	2300	0.27
<i>Chilotherium kowalevskii</i>	Ch. k.	700	0.36
<i>Coelodonta antiquitatis</i>	Co. a.	2402	0.29
<i>Coelodonta nihowanensis</i>	Co. n.	NA	0.24
<i>Diaceratherium aginense</i>	Dia. ag.	1987	0.31
<i>Diaceratherium asphaltense</i>	Dia. as.	NA	0.31
<i>Diaceratherium aurelianense</i>	Dia. au.	1551	0.38
<i>Diaceratherium lemanense</i>	Dia. le.	1590	0.30
<i>Diceratherium armatum</i>	Dm. ar.	NA	0.21
<i>Diceratherium tridactylum</i>	Dm. t.	517	0.25
<i>Dicerorhinus sumatrensis</i>	Ds. su.	775	0.27
<i>Diceros bicornis</i>	Dc. b.	1050	0.27
<i>Dihoplus megarhinus</i>	Dh. m.	NA	0.27
<i>Dihoplus pikermiensis</i>	Dh. p.	1100	0.28
<i>Dihoplus schleiermacheri</i>	Dh. s.	2122	0.26
<i>Elasmotherium sibiricum</i>	E. s.	4500	0.24
<i>Hoploaceratherium tetradactylum</i>	Ho. t.	1197	0.26
<i>Hyrachyus eximius</i>	Hy. e.	67	0.17
<i>Hyrachyus modestus</i>	Hy. m.	NA	0.16
<i>Hyracodon nebraskensis</i>	Hn. n.	NA	0.16
<i>Lartetotherium aff. sansaniense</i>	Ds. sa.	NA	0.25
<i>Lartetotherium sansaniense</i>	L. s.	1204	0.24
<i>Menoceras arikareense</i>	Mc. a.	313	0.17
<i>Metamynodon planifrons</i>	Md. p.	1340	0.34
<i>Nesorhinus philippinensis</i>	N. p.	1086	0.28
<i>Paraceratherium grangeri</i>	Pa. g.	10950	0.24
<i>Peraceras hessei</i>	Pe. h.	NA	0.26
<i>Peraceras profectum</i>	Pe. p.	NA	0.26
<i>Plesiaceratherium mirallesi</i>	Pl. m.	1268	0.25
<i>Pleuroceros blanfordi</i>	Pc. b.	1343	NA
<i>Prosantorhinus douvillei</i>	Ps. d.	NA	0.45
<i>Protaceratherium minutum</i>	Pt. m.	530	0.22
<i>Rhinoceros sondaicus</i>	R. s.	1350	0.35
<i>Rhinoceros unicornis</i>	R. u.	2000	0.27
<i>Stephanorhinus jeanvireti</i>	St. j.	NA	0.23
<i>Stephanorhinus etruscus</i>	St. e.	NA	0.24
<i>Stephanorhinus hemitoechus</i>	St. he.	1561	0.26
<i>Subhyracodon mitis</i>	Su. m.	NA	0.26
<i>Subhyracodon occidentalis</i>	Su. o.	NA	0.24
<i>Teleoceras fossiger</i>	Te. f.	1016	0.44
<i>Teleoceras hicksi</i>	Te. h.	1660	0.46

<i>Teleoceras proterum</i>	Te. p.	635	0.43
<i>Trionias osborni</i>	Tg. o.	505	0.22
<i>Trionias wellsii</i>	Tg. w.	NA	NA
<i>Urtinotherium intermedium</i>	U. i.	NA	0.23

---

1652

1653

1654 **Table 2.** Results of the Pearson's correlation tests between centroid size (CS), and mean body mass  
 1655 (BM) and mean gracility index (GI-MT3) respectively for each bone (computed on Phylogenetic  
 1656 Independent Contrasts). **r**: Pearson's correlation coefficient value; **t**: student distribution value; **dF**:  
 1657 degrees of freedom; **p**: p-value. Significant results (for  $p < 0.01$ ) are indicated in bold.

<b>Bone</b>	<b>Variables</b>	<b>r</b>	<b>t</b>	<b>dF</b>	<b>p</b>
Femur (complete)	<b>CS ~ BM</b>	<b>0.70</b>	<b>4.72</b>	<b>23</b>	<b>&lt;0.01</b>
	CS ~ GI	0.15	0.91	36	0.37
Femur (proximal partial)	<b>CS ~ BM</b>	<b>0.91</b>	<b>10.44</b>	<b>24</b>	<b>&lt;0.01</b>
	CS ~ GI	0.22	1.36	38	0.18
Femur (distal partial)	<b>CS ~ BM</b>	<b>0.86</b>	<b>8.46</b>	<b>26</b>	<b>&lt;0.01</b>
	CS ~ GI	0.16	0.99	40	0.32
Tibia	<b>CS ~ BM</b>	<b>0.72</b>	<b>5.23</b>	<b>26</b>	<b>&lt;0.01</b>
	CS ~ GI	-0.23	-1.51	39	0.14
Fibula	<b>CS ~ BM</b>	<b>0.71</b>	<b>4.46</b>	<b>20</b>	<b>&lt;0.01</b>
	CS ~ GI	-0.28	-1.41	24	0.17

1658

1659

1660 **Table 3.** Range of R<sup>2</sup> and p-values for PGLS computed with NNI permuted trees on shape data and  
 1661 log-transformed centroid size (CS), log-transformed cubic root of mean body mass (BM) and log-  
 1662 transformed mean gracility index (GI-MT3). **N:** number of trees obtained after NNI procedure; **R<sup>2</sup>:**  
 1663 determination coefficient value. Significant results (for mean p < 0.01) are indicated in bold.

Bone	Variable	N	R <sup>2</sup>			p-value		
			Min.	Max.	Mean	Min.	Max.	Mean
Femur (complete)	CS	76	<b>0.06</b>	<b>0.10</b>	<b>0.07</b>	<b>0.001</b>	<b>0.022</b>	<b>0.003</b>
	BM	46	<b>0.14</b>	<b>0.23</b>	<b>0.16</b>	<b>0.001</b>	<b>0.005</b>	<b>0.002</b>
	GI	74	<b>0.06</b>	<b>0.07</b>	<b>0.09</b>	<b>0.001</b>	<b>0.011</b>	<b>0.003</b>
Femur (proximal partial)	CS	80	<b>0.05</b>	<b>0.11</b>	<b>0.07</b>	<b>0.001</b>	<b>0.015</b>	<b>0.004</b>
	BM	48	<b>0.08</b>	<b>0.11</b>	<b>0.11</b>	<b>0.001</b>	<b>0.016</b>	<b>0.002</b>
	GI	78	<b>0.05</b>	<b>0.07</b>	<b>0.06</b>	<b>0.001</b>	<b>0.030</b>	<b>0.009</b>
Femur (distal partial)	CS	86	0.06	0.07	0.06	0.017	0.051	0.033
	BM	52	0.07	0.10	0.08	0.042	0.182	0.095
	GI	82	<b>0.06</b>	<b>0.08</b>	<b>0.07</b>	<b>0.002</b>	<b>0.025</b>	<b>0.011</b>
Tibia	CS	82	0.04	0.06	0.04	0.040	0.119	0.082
	BM	52	<b>0.08</b>	<b>0.18</b>	<b>0.13</b>	<b>0.004</b>	<b>0.048</b>	<b>0.009</b>
	GI	80	<b>0.22</b>	<b>0.31</b>	<b>0.27</b>	<b>0.001</b>	<b>0.001</b>	<b>0.001</b>
Fibula	CS	52	0.05	0.10	0.08	0.018	0.267	0.046
	BM	42	0.03	0.11	0.08	0.051	0.0.597	0.146
	GI	50	<b>0.17</b>	<b>0.22</b>	<b>0.20</b>	<b>0.001</b>	<b>0.003</b>	<b>0.001</b>

1664

1665 **SUPPLEMENTARY DATA**

1666 **Table S1:** Complete list of all the studied specimens.

1667 **Figure S1** Summary of the anatomical areas of the rhino long bone. Bones figured here belong to *C.*

1668 *simum*. **A: Humerus. Abbreviations** – F.c.: Fovea capitis; G.t.: Greater trochanter; G.t.c.: Greater  
1669 trochanter convexity; G.t.t.: Greater trochanter top; H.: Head; I.s.: Intercondylar space; L.c.: Lateral  
1670 condyle; L.e.: Lateral epicondyle; L.t.r.: Lateral trochlear ridge; L.t.: Lesser trochanter; M.c.: Medial  
1671 condyle; M.e.: Medial epicondyle; M.t.r.: Medial trochlear ridge; N.: Neck; S.f.: supracondylar fossa;  
1672 T.: Trochlea; T.f.: Trochanteric fossa; T.g.: Trochlear groove; T.t.: Third trochanter. **B: Tibia.**

1673 **Abbreviations** – A.s.t.: Articular surface for the talus; C.a.: Caudal apophysis; Ce.i.a.: Central  
1674 intercondylar area; Cr.i.a.: Cranial intercondylar area; D.a.s.f.: Distal articular surface for the fibula;  
1675 E.g.: Extensor groove; I.c.: Interosseous crest; L.a.s.: Lateral articular surface; L.c.: Lateral condyle;  
1676 L.g.: Lateral groove; L.i.t.: Lateral intercondylar tubercle; M.a.s.: Medial articular surface; M.c.: Medial  
1677 condyle; M.g.: Medial groove; M.i.t.: Medial intercondylar tubercle; M.m.: Medial malleolus; P.a.s.f.:  
1678 Proximal articular surface for the fibula; P.n.: Popliteal notch; S.s.m.p.: Sliding surface for the m.  
1679 popliteus; T.c.: Tibial crest; T.g.: Tuberosity groove; T.t.: Tibial tuberosity. **C: Fibula. Abbreviations** –  
1680 A.s.t.: Articular surface for the talus; Ca.l.: Caudo-lateral line; Ca.t.l.m.: Caudal tubercle of the lateral  
1681 malleolus; Cr.l.: Cranio-lateral line; Cr.t.l.m.: Cranial tubercle of the lateral malleolus; D.a.s.t.: Distal  
1682 articular surface for the tibia; D.g.m.: Distal groove of the malleolus; H.: Head; I.c.: Interosseous crest;  
1683 L.g.: Lateral groove; P.a.s.t.: Proximal articular surface for the tibia.

1684 **Data S1:** Designation and location of the anatomical landmarks placed on each bone.

1685 **Table S2:** Complete list of gracility index and mean body mass compiled from literature.

1686 **Table S3:** Summary of the differences in  $p$  and  $R^2$  values between the PGLS computed under a  
1687 Brownian Motion (BM) model (geomorph) and a Ridge Regression (RR) model (RRphylo). Only  
1688 variables with significant results are presented here.

1689 **Figure S2:** Shape deformations associated with the first two axes of the PCA for each bone. Blue:  
1690 minimal values. Orange: maximal values. Orientation from left to right: caudal, lateral, cranial,  
1691 medial, proximal and distal views. **A:** complete femur; **B:** proximal partial femur; **C:** distal partial  
1692 femur; **D:** tibia; **E:** fibula.

1693 **Figure S3:** Shape deformations associated with minimum and maximum values of the centroid size  
1694 (CS), body mass (BM) and gracility index (GI-MT3) for significant regressions with shape. Blue:  
1695 minimal values. Orange: maximal values. Orientation from left to right: caudal, lateral, cranial,

1696 medial, proximal and distal views. **A, B, C:** complete femur; **D, E, F:** proximal partial femur; **G:** distal  
1697 partial femur; **H, I:** tibia; **J:** fibula.

1698 **Figure S4.** Significant PGLS regression plots for distal partial femur (**A**) and fibula (**B**) performed on  
1699 shape data and log-transformed centroid size (CS) or log-transformed cubic root of mean body mass  
1700 (BM). Points colour code follows Figure 1. Point size is proportional to mean log CS of each species.  
1701 On the right, shapes associated with minimum and maximum fitted values (top row) and colour maps  
1702 of the location and intensity of the shape deformation (bottom row). Blue: minimal values. Orange:  
1703 maximal values. For each bone, the shape associated with the minimum was coloured depending on  
1704 its distance to the shape associated with the maximum (blue indicates a low deformation intensity  
1705 and red indicates a high deformation intensity). Orientation from left to right in each case: caudal,  
1706 lateral, cranial and medial views.

1707 **Figure S5:** Boxplot of the distribution of GI-MC3 (from Mallet et al., in press) and GI-MT3 values (this  
1708 work). Parametric tests indicate a very high correlation between the two indices, and a very high  
1709 probability of similar mean and variance.